



Design methodology for multi-parallel pipe separator (MPPS)

Hamidreza Asaadian ^{*}, Milan Stanko

Department of Geoscience and Petroleum, Norwegian University of Science and Technology, Trondheim, Norway

ARTICLE INFO

Keywords:

Multi-parallel pipe separator
Droplet size Distribution
Oil-water separation, Batch dispersion-separation model
Drainage potential curve

ABSTRACT

The Multiple Parallel Pipe Separator (MPPS) is a design for bulk oil-water separation that utilizes multiple horizontal pipe segments connected in parallel. Drainage of water is performed through tapping points on the pipe's bottom. Pipe segments can be added in series (stacked) if needed. The aim of this study is to develop a design methodology for the MPPS that can be adapted to varying flow conditions.

The methodology employs different types of models: flow pattern, drainage potential curves, and oil-water dispersion in pipe. The flow pattern model is used to determine the number of branches and pipe diameter to ensure segregated flow patterns. The batch dispersion-separation model is used to predict the thickness of the water oil and dispersion layers approaching the tapping point. The drainage potential model is used to determine tapping point separation performance and the number of required tapping points. All models are validated with experimental data available from previous and current experimental campaigns with inlet water cut, WC_{inlet} , from 30 % to 90 % and total flow rate from 300 to 700 L/min.

The results indicate that when the flow is oil-continuous (e.g., with an WC_{inlet} of 30 %) and the mixture velocity is high (e.g., 0.33 m/s), the droplet coalescence is limited, and the change of the emulsion layer thickness is less than 14 % of initial emulsion thickness. However, if the number of parallel branches is increased, the mixture velocity decreases, and consequently the residence time becomes longer enough to facilitate dissolving the emulsion layer. Furthermore, when the inlet water cut is low (e.g., 30 %), increasing the number of tapping points assists in extracting the water phase with a higher water cut. Conversely, when the inlet water cut is higher (e.g., 60 %), achieving a moderate water cut requires fewer tapping points.

1. Introduction

The water content of produced reservoir fluids from deep-sea fields is constantly rising with time, and most of the water treatment systems on platforms have reached their maximum capacity (Bowers et al., 2000). To address this challenge, an alternative is to separate the growing amounts of water from the hydrocarbons on the seabed. The implementation of this technology could prolong the profitability of the oil fields and also keep the reservoir pressure constant (Shi et al., 2012).

Normally, produced water is delivered along with the production stream to the topside, where it is separated and cleaned. The water is then either reinjected for pressure support or disposed of in the sea, depending on the facility. Increased produced water rates eventually pose problems for offshore installations, particularly when the lifespan of the facilities exceeds the design specification. This is a relatively common occurrence (da Silva et al., 2013). Produced water production will increase as a field matures, eventually exceeding the design capacity and bottlenecking production. Subsea separation of produced water

allows topside facilities to be de-bottlenecked, allowing for higher production rates and new tie-ins to existing facilities (Skjefstad and Stanko, 2017). Although subsea separation is appealing, more research into separator structure optimization is required to avoid excessive deployment and installation costs of large components subsea.

Concerning bulk oil-water separation, the pipe separator concept uses a small diameter and a short residence time. The separation is effective because water and oil are transported over a shorter vertical distance due to the small pipe diameter. A shear force is created at the interface between the oil and water phases due to the difference in flow speed. This breaks up the oil and water emulsion. The pipe has a horizontal flow, which prevents emulsion building up in the separator (Sagatun et al., 2008, May).

Recently, an innovative separator design that relies on separation in multiple pipes rather than vessels was designed and built by (Skjefstad and Stanko, 2018). This separator is called the Multiple Parallel Pipe Separator (MPPS). Similar to the pipe separator, the MPPS is more suitable than conventional vessel-type separators for installation in deeper seas due to the smaller diameter of the pipes. Fig. 1 illustrates the

* Correspondence to: S. P. Andersens veg 15a, 7031 Trondheim, Norway.

E-mail addresses: hamidreza.asaadian@ntnu.no, hamidreza.asaadian@hotmail.com (H. Asaadian).

Nomenclature		
<i>A</i>	area, m ²	<i>v_s</i> slip velocity, m/s
<i>Ar</i>	Archimedes number	<i>w</i> Width, m
<i>B_O</i>	Oil formation volume factor, bbl/stb	<i>α</i> Phase fraction
<i>C_W</i>	friction coefficient	<i>α_{D/C}</i> phase contamination
<i>D</i>	diameter, m	<i>ρ</i> density, kg/m ³
<i>ER</i>	extraction rate	<i>ϕ</i> dispersed phase fraction
<i>K_{HR}</i>	Hadamard-Rybczynski factor	<i>λ</i> settling velocity parameter
<i>L</i>	length, m	<i>μ</i> viscosity, Pa.s
<i>La</i>	modified Laplace number	<i>ξ</i> settling velocity parameter
<i>Q</i>	flowrate, m ³ /s	<i>τ_C</i> droplet/droplet coalescence time
<i>Re_∞</i>	Reynolds number of a single droplet in an infinite fluid	<i>τ_I</i> droplet/interface coalescence time
<i>V_S</i>	settling velocity, m/s	<i>σ</i> interfacial tension, mN/m
<i>WC</i>	water cut	<i>φ</i> cumulative frequency
<i>WT</i>	water tapped	<i>Subscripts</i>
<i>d</i>	diameter, m	C continuous phase or layer
<i>d₃₂</i>	Sauter mean diameter, m	D dispersed phase or layer
<i>g</i>	gravity, m/s ²	E Emulsion
<i>h</i>	layer thickness, m	O Oil
<i>u</i>	axial velocity, m/s	P Particle
<i>r_a</i>	radius of the channel contour, m	W Water
<i>r_{F,C}</i>	radius of the droplet/droplet contact area, m	i Initial
<i>r_{F,I}</i>	contact area radius, m	m Mixture
<i>r_v[*]</i>	dimensionless asymmetry of the film drainage parameter	res Residence
<i>t</i>	time, s	t Total

MPPS concept design.

The MPPS consists of multiple horizontal pipe segments connected in parallel. The inlet (1) is a T-section header that divides the incoming production stream into branch streams. The inlet is tangential, and it is designed to improve separation by centrifugal forces and avoiding mixing. The heavier phase will be pushed towards the pipe wall, while the lighter phase will concentrate in the center of the pipe. Extraction points located in the upper section of the descending pipes are connected to ascending pipes to facilitate gas removal (2). Downstream the inlet, there are internals at the start of each branch that change the fluid distribution from a core-divided phase distribution to a stratified flow arrangement upstream of the connected descending portion (3). Downstream from the inlet section, the flow progresses into a horizontal mid-section where the bulk of the liquid-liquid separation occurs, driven

by gravitational forces and variations in density (4). The horizontal pipe segments are followed by extraction sections (5). Water (w) extraction is carried out in an inclined extension of the horizontal pipes, where water is slowed down, providing a large hold up and low velocities for a smooth extraction. The residual oil-rich stream flows up and down the sloped portion for separate extraction (o). The extraction section is designed in such a way that numerous horizontal pipe sections can be placed in sequence without expanding the areal footprint of the separator. All extraction pipelines are linked to a shared outlet, one for water and one for oil, ensuring a system with self-regulation ([Skjefstad and Stanko, 2019](#)).

[Skjefstad and Stanko \(2017\)](#) investigated their proposed MPPS concept design from various perspectives such as weight reduction, capacity estimation, and performance analysis. Their study revealed that

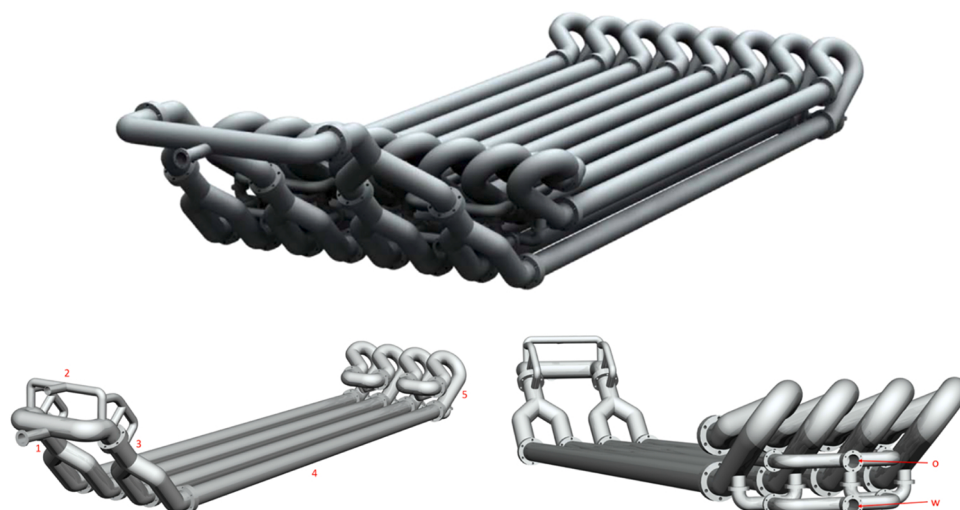


Fig. 1. Initial MPPS design concept ([Skjefstad & Stanko, 2018](#)).

the separator demonstrated favorable separation efficiencies (>98 %) for both oil and water continuous inlet flow streams with low to moderate mixture flow velocities. Furthermore, the authors evaluated the separation performance of the MPPS by altering certain geometric features of the separator, such as the inlet configuration and the location of the drained water tapping point (Skjefstad et al., 2020). Their findings suggested that utilizing a tangential inlet configuration with some internals in the T-section resulted in even phase splitting in each branch, better phase separation, and by positioning the tapping point closer to the bottom of the ascending pipe section this resulted in higher separation efficiency (Skjefstad and Stanko, 2019). In a subsequent study, Asaadian et al. (2022) addressed gaps in the existing research by describing the performance of the tapping point in the MPPS separator in the form of a drainage potential curve. This model showed fair agreement with the experimental data. They also added small amounts of crude oil to the model oil to approximate the separation characteristics of the real crude oil-saltwater fluid system. In another study, they examined how the efficiency of the separator, and the drainage potential curves were impacted by the introduction of a small amount of gas (Asaadian & Stanko, 2023).

The objective of this study is to provide a method to perform a preliminary design of the MPPS that adapts to varying flow conditions, such that the ones exhibited when producing reservoir fluids during the lifetime of a field. To this goal, reliable models and methods are presented to predict the separation process along the horizontal section and provide input for the drainage tapping point model (i.e., drainage potential curve). These models and methods are validated through experimental data. This study also showcases different design cases and how the design concept varies depending on various flow conditions. The developed methods and models justify the geometry configuration of MPPS, such as the number of branches, number of stacks, and the pipe diameter. Additionally, this study offers a comprehensive design methodology for the MPPS and applies its workflow to a real case study. This will help advance the technology readiness level of the MPPS.

The research introduces several innovative methodologies and contributions that significantly advance the current understanding and practical applications in the field. Firstly, the MPPS model-based design methodology represents a novel approach, offering a systematic framework for the optimization of multiphase pipe separation systems. This methodology stands out from prior models by providing a more comprehensive and adaptable tool for designing efficient separation processes. Secondly, the development of the batch dispersion-separation model is a significant breakthrough, as it accurately predicts the evolution of oil, water, and dispersion layers in horizontal pipe sections. This model enhances the precision of separation processes, surpassing previous predictive models which often lacked the capability to dynamically account for the complexities of fluid behavior in pipelines. Thirdly, the customization of the model from previous works for designing the required number of tapping points in the MPPS and determining their operational conditions introduces a practical and tailored solution for real-world applications. This aspect of the research bridges the gap between theoretical models and practical implementation, facilitating the design of more efficient and effective separation systems. Lastly, the efforts to increase the Technology Readiness Level (TRL) of the MPPS are particularly noteworthy (Assar et al., 2024). By advancing the TRL, this research not only contributes to the theoretical understanding but also brings the technology closer to industrial application, ensuring that it can be reliably used in practical settings. Collectively, these contributions significantly enhance the existing body of knowledge and offer practical tools and methodologies that are directly applicable in the industry, setting a new standard for future research and development in multiphase pipe separation systems.

2. Method

Several geometric properties must be determined for the MPPS, such

as: 1. the pipe diameter (ID), 2. the number of parallel branches and 3. Number of series stacks. In this work it is considered that the length of the pipe separator is fixed (around 6–7 m) to allow installation by a larger fleet of offshore installation vessels (Skjefstad and Stanko, 2017). To define the design parameters of the MPPS, the steps shown in Fig. 2 are proposed. Some of the models used in the method described in Fig. 2 will be discussed in detail next.

2.1. Reservoir production history and forecast (Step 1)

The total flow rate, water cut, and fluid properties are extracted from the forecasted production profile of the field and the design basis. The dimensions of the separator will be directly influenced by the total flow rate and water cut.

2.2. Pattern map of oil/water flow in horizontal pipe (Step 2)

The flow regime of oil/water in a horizontal pipe can be described by a flow pattern map, which depicts the various flow patterns that occur under specific flow conditions. To achieve efficient water separation by MPPS, it is desirable to have a stratified flow or other flow patterns that feature a clean water layer. The thickness and the stability of the emulsion layer will affect the separation efficiency of the MPPS. Modifying the pipe diameter and number of branches can help to obtain more separation-favorable flow patterns in the MPPS. Increasing the number of parallel branches and the pipe diameter results in lower mixture velocity and the formation of segregated patterns. Horizontal oil/water flow can exhibit various flow-pattern configurations, as classified by Trallero (1995) for fully developed oil/water flow in horizontal pipes (see Fig. 3).

1. Stratified flow (ST): The ST flow pattern is characterized by two liquid layers, with water typically at the bottom and oil at the top due to their respective densities.
2. Stratified flow with interface mixing (ST and MI): The ST and MI flow pattern tends to be stratified but has an unstable interface, which creates a mixing zone. Although there is significant mixing at the interface, the top and bottom of the pipe still contain pure fluids.
3. Dispersion of oil in water with a water layer (DO/W and W): The DO/W and W flow pattern features dispersed oil droplets flowing on the top while clear water flows on the bottom.
4. Dispersion of oil in water (DO/W): In the DO/W flow pattern, water containing dispersed oil droplets fills the entire cross-sectional area of the pipe.
5. Dispersion of water in oil (DW/O): In the DW/O flow pattern, water is present as droplets throughout the entire cross-sectional area of the pipe, with oil acting as the continuous phase.
6. Dual dispersion (DO/W and W/O): This flow pattern contains two distinct layers. Both phases are present throughout the entire pipe, with oil that contains water droplets being the continuous phase on the top and water being the continuous phase on the bottom, with dispersed droplets of oil present.

2.3. Batch dispersion-separation model (Step 3)

To assess the performance of the separation process in the horizontal section and provide input to the tapping point performance model, a reliable model is required to predict the thickness of each phase and the amount of contamination along the horizontal section of the MPPS. The separation process is dominated by gravity due to the low liquid velocities and the momentum of the continuous phase is also low. To approximate the behavior of the horizontal section of the MPPS, an extension of the batch dispersion-separation process can be employed. Batch dispersion-separation models are capable of predicting the development of the separation profiles over time. However, these models assume that both phases move at the same velocity as the mixing

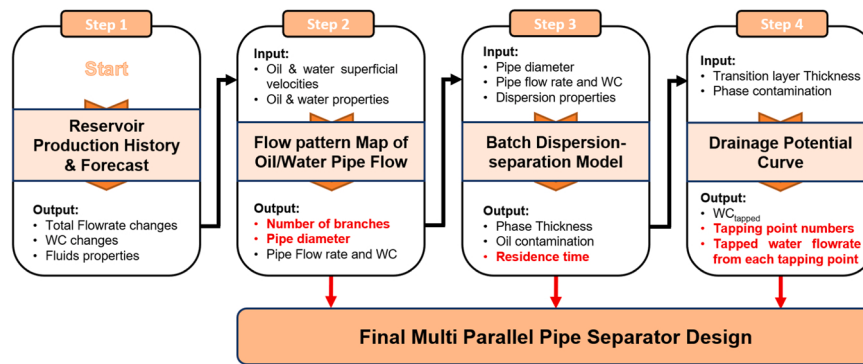


Fig. 2. Design methodology for the MPPS.

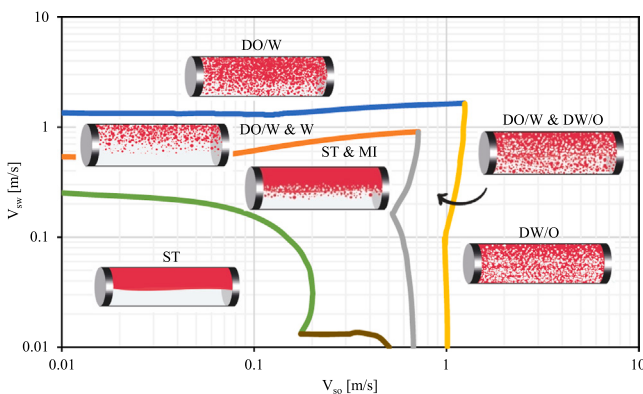


Fig. 3. Flow pattern map of oil/water pipe flow (Trallero, 1995).

velocity, thereby ignoring any impact that the velocity profile and momentum exchange might have on droplet coalescence between layers. These models can be expanded to the MPPS by considering this assumption.

Among the various theories for predicting batch dispersion-separation behavior, the asymmetric dimple model proposed by Henschke et al. (2002) was deemed to be the most suitable for application to the MPPS. Because the fluid film lacks angular symmetry, causing an asymmetric drainage concerning the contact area's normal axis (Hartland, 1969; Burrill and Woods, 1973). Besides, the model of Henschke et al. (2002) allows to include this effect by including a calibration of the asymmetry parameter r_V^* . Henschke et al. (2002) noted that the r_V^* parameter remains unaffected by the initial droplet-size distribution, water cut, or batch height for a given oil/water mixture. This flexibility allows straightforward scaling up of a bottle test to actual field conditions. Additionally, by converting the timescale in the batch separator to space and incorporating the average oil/water mixture velocity U_m , the batch dispersion-separation model can be expanded to account for pipe flow in the MPPS. Fig. 4 shows the separation profile of oil-water pipe flow in a horizontal pipe.

Other mechanistic models for predicting separation in pipes rely on two submodels: the hydrodynamic model and the coalescence model. The hydrodynamic model considers momentum transfer among three

layers: the water continuous, dense-packed, and oil continuous layers. The coalescence model uses a simplified population balance equation to account for droplet evolution in the dense-packed zone. These models require several coalescence parameters of the oil/water mixture that cannot be obtained from simple tests. The proposed model, however, provides a simplified approach that allows these coalescence parameters to be determined through straightforward experimental tests (Hartland, 1967a, 1967b, 1967c; Hartland and Jeelani, 1988).

The basic assumptions of this model are as follows:

1. Mono dispersion (uniform droplet size at any given time and position).
2. A clear interface or a negligible impact from surface agents.
3. Asymmetric draining of the film.

The separation profile is predicted by determining interfaces between clean saltwater, oil and emulsion layers. As it is illustrated in Fig. 5, these layers are named as the single-phase oil and water layers, h_o and h_w , dense-packed h_p , and sedimentation h_s layers. More details about the batch dispersion-separation model and the solving process are provided in Appendix A.

The phase contamination is referred to as the fraction of dispersed phase that remains when some droplets are unable to reach the interface and instead remain in the continuous phase. Emulsions are unstable systems that naturally separate over time, reducing the interfacial area between the oil and water phases. In a gravitational setting, dispersed droplets experience a vertical force caused by differences in density between the continuous and dispersed phases (Mandal et al., 2017). This force is counteracted by the buoyancy force and fractional drag force, which balance out the gravitational pull. The resulting settling rate (V_s) for a single droplet is described by Eq. 1, commonly referred to as Stokes' law (Stokes, 1851).

$$V_s = \frac{(\rho_d - \rho_c)gd^2}{18 \mu_c} \quad (1)$$

With known total flowrate (\dot{Q}_w), cross sectional area of pipe (A_c), and effective length of the horizontal section (L_{eff}), the residence time (t_{res}) is given by:

$$t_{res} = L_{eff} / (\dot{Q}_w / A_c) \quad (2)$$

The lowest size of the dispersed droplets which are able to reach the interface during a specific residence time is called critical droplet size in this work. The critical droplet size of the segregated pipe segments increases from the bottom of the pipe to the interface. The critical droplet size (d_c) for each pipe segment from the bottom to the interface, which is shown in Fig. 6, is defined as:

$$d_c = \sqrt{\frac{18 \mu_c (h_s - h_i)}{\Delta \rho g t_{res}}} \quad (3)$$

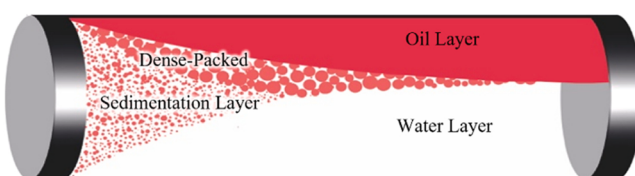


Fig. 4. Separation process in oil-water flow.

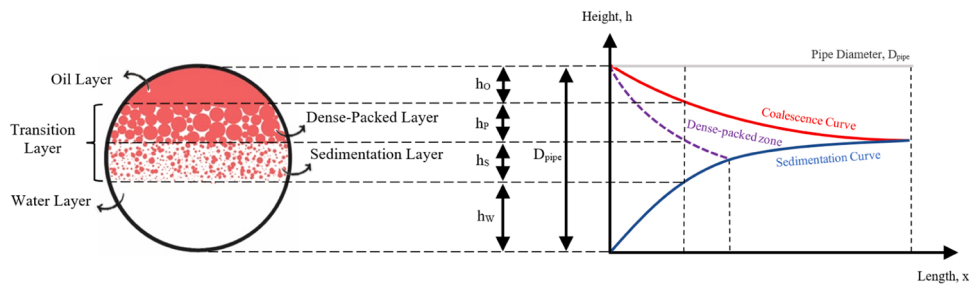


Fig. 5. Separation profile for water continuous dispersion flow in pipe.

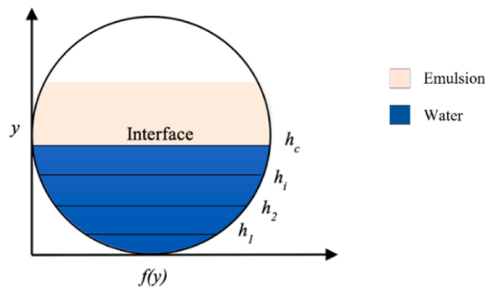


Fig. 6. Cross-section segments in the water layer.

Where μ_c is continuous phase viscosity and $\Delta\rho$ is phase density difference. If the critical droplet size is smaller than the minimum droplet diameter of the dispersed phase, it means there is no phase contamination ($\alpha_{D/C}$). If this is not the case, the phase contamination is given by:

$$\alpha_{D/C} = \int_0^{h_c} w(y) \alpha_D \varphi_o(d_c) dy \quad (4)$$

where $w(y)$ is the width of the segment, α_D is the initial dispersed fraction and $\varphi_o(d)$ is the cumulative frequency of the droplet size distribution.

2.4. Drainage potential model (Step 4)

The drainage potential of the pipe refers to the amount of water being tapped at the bottom or tapping point in the pipeline relative to the water cut of the tapped stream. Stanko & Golan (2015) defined a drainage potential curve as the relationship between WC_{tapped} and the tapping point efficiency, Water Tapped (WT). WT is defined as the ratio of tapped water flow to the inlet water flow.

$$WT[\%] = \frac{\dot{Q}_{\text{water tapped}}}{\dot{Q}_{\text{water}}} \cdot 100 \quad (5)$$

A number of factors influence this relationship, including the oil and water flow rates and characteristics, pipe size, inclination, and material, as well as the positioning and design of the tap. Asaadian et al. (2022) developed a simplified model for predicting potential curves based on the overall flow rates, water cuts, thickness of the transition zone (emulsion layer), and phase contamination levels. Additional information on the model and its fundamentals can be found in Asaadian et al. (2022). The model produces a drainage potential curve as an outcome when provided with the specific input mentioned. Fig. 7 displays the drainage potential curve produced by the model due to the specified inputs such as inlet water cut, pipe diameter, dispersion phase distribution in emulsion layer and total flow rate. The curve in Fig. 7 shows that it is possible to drain 40 % of the total water flow by the tapping point without any oil contamination and after that the more tapped water flow, the more oil contamination appears. Finally, draining the whole water flow results in a 35 % oil fraction (65 % WC_{tapped}). Multiple

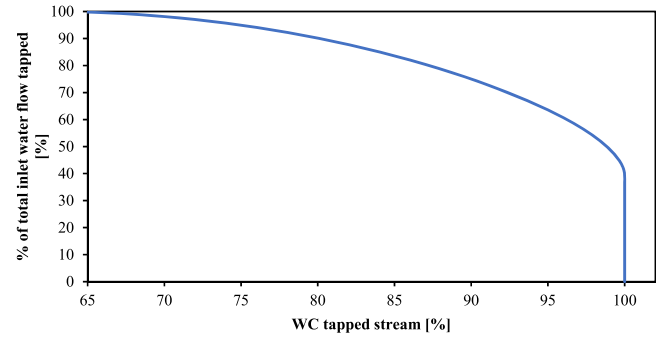


Fig. 7. Drainage potential curve.

tapping points design that has stacks in series and a possible tapping point at the end of the horizontal section of each stack is a potential solution to transfer the oil rich stream to the next tapping point for draining more saltwater with lower oil contamination.

2.5. Model verification and tuning using the multi-parallel pipe separator (MPPS) prototype

The multiphase flow loop developed and used by Skjefstad and Stanko (2019), is utilized in this study to test and calibrate the models described above for prediction of separation performance of the MPPS. Experimental campaigns have been conducted at the Department of Geoscience and Petroleum at NTNU. Since the separator is built with transparent DN65 PVC pipes, it is possible to measure the evolution of the different layers in the separator using rulers glued to the outer part of the pipe.

The MPPS prototype is designed and built according to the same configuration that is discussed in the Introduction section. Among the major components of this experimental setup are a storage tank and pumping system, an inlet metering section, a mixing section, a separation concept, an outlet metering and control section and a data logging and control system which are illustrated in Fig. 8. Before water and oil are mixed, two Micro Motion F200 mass flowmeters are used to measure their flow rates and densities (DT.1, FT.1, DT2, FT.2). Mixing a mixture of oil and water is done in a mixing tee. The oil outlet is connected directly to the main tank. The water outlet is first metered by a mass flowmeter (DT3, FT3) and then returned to the main tank to close the test loop. Two control valves (VT.1, VT.2) which are installed on outlets control the rate of extraction. The inlet total flowrate and water cut have been adjusted to the changing frequency of pumps by a data logging and control system.

The MPPS body is made of transparent PVC pipe with a 152.4 mm ID and 6.1 m length. Mixture inlet and oil and water outlet pipes have a diameter of 76.2 mm. Three sampling points (SP.1, SP.2, SP.3) are proposed at the inlet pipe and at the beginning and end of the horizontal section before the tapping point. These sampling points are designed to take sample from the transition layer to measure the water cut of the

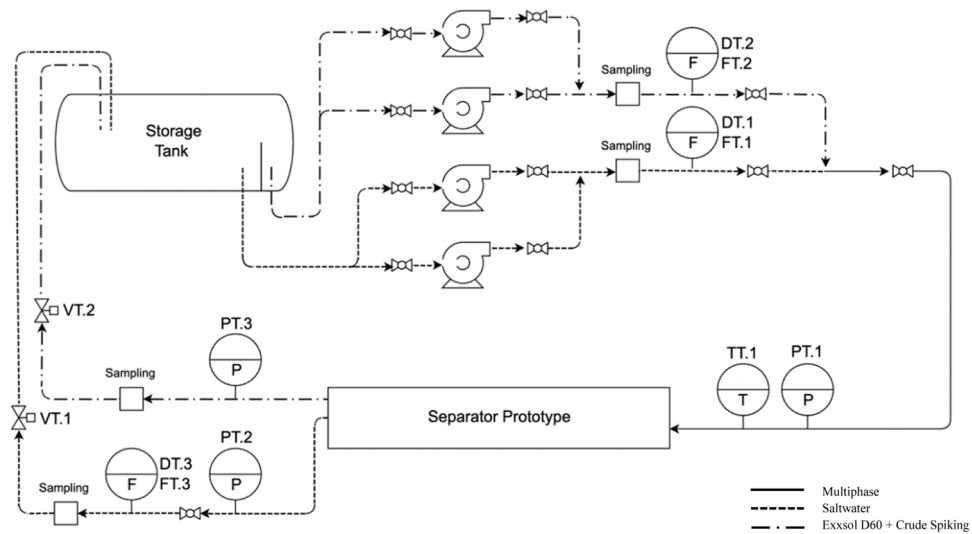


Fig. 8. P&ID diagram of MPPS.

emulsion layer. More details about the sampling points are given in the Appendix B. The Mettler Toledo PVM V819 probe is also utilized to record microscopic images from the emulsion layer through the sampling points. To obtain a precise measurement of the water cut and droplet size distribution in the transition layer between the oil and water layers, sampling and PVM probes are placed in the middle of the emulsion layer. Real-time droplet size measurement is provided by images taken with the PVM probe. Four visualization sections (VS.1, VS.2, VS.3, VS.4) are marked along the transparent horizontal pipe to measure the thickness of the water and oil layers using cameras (refer to Fig. 9). The pipe curvature is accounted for when interpreting measurements from the recorded images. Unfortunately, when using visual observation alone it is not possible to identify the interface between the dense-packed zone and the sedimenting region. Consequently, this study did not measure the thickness of the dense-packed zone.

Distilled water with 3.4 wt% NaCl and mineral oil Exxsol D60 spiked with 400 ppm crude oil and 0.015 gr/L Oil Red O ($C_{26}H_{24}N_4O$) was used to mimic the real saltwater-crude fluid system and provide easier phase distinction. The oil has a density of 796.2 kg/m^3 (at 15°C), viscosity of 1.41 cP, and interfacial tension of 28.8 mN/m (Asaadian & Stanko, 2023). The experiment was conducted under steady-state, stratified flow-pattern conditions, with various inlet water cuts (WC_{inlet}) of 30 %,

50 %, 70 %, and 90 % evaluated at the mixture flow rates of 300, 500, and 700 L/min (equivalent to 0.14, 0.21, and 0.33 m/s mixture velocity in each pipe branch). Table 1 presents the test range in terms of inlet flow rate and water cut extraction rate (ER) and investigation points for each implemented methods in this study. The results of the experiment and model were estimated and reported at fixed extraction rates (ER), which were calculated using Eq. 6. This equation divides the flow rate through the water return/extraction line (Q_3) by the mixed incoming flow rate through the water feed line (Q_1).

$$ER = \frac{Q_3}{Q_1} \quad (6)$$

3. Results

This section is split into the following parts: Firstly, the impact of the number of branches on the flow pattern in the horizontal part of the separator is investigated using a flow pattern map taken from the literature. Secondly, the results of the experimental campaign are presented, describing the evolution along the horizontal section of the layer thicknesses, water cut, and droplet size distribution of the emulsion layer. These values are relevant for tuning the batch dispersion-

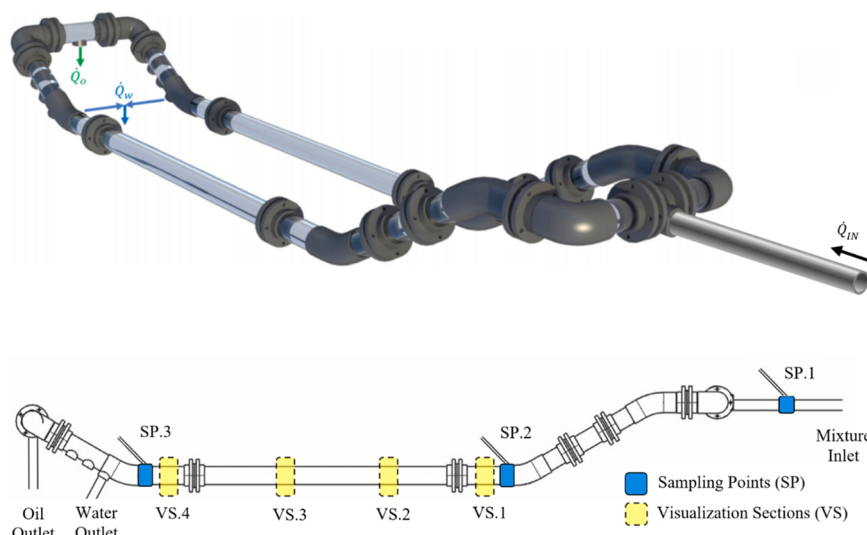


Fig. 9. MPPS experimental prototype.

Table 1
Test matrix.

Exp. Inputs			Methods Investigation Points			
Q _t [L/min]	WC _{inlet} [%]	ER [%]	Phases thickness	Emulsion water cut	Droplet size distribution	Batch dispersion-separation model validation
300	30/50/70/90	90	VS1/VS2/VS3/VS4	SP1/SP2/SP3	SP1/SP2/SP3	-
500	30/50/70/90	90	VS1/VS2/VS3/VS4	SP1/SP2/SP3	SP1/SP2/SP3	-
700	30/50/70	90	VS1/VS2/VS3/VS4	SP1/SP2/SP3	SP1/SP2/SP3	-
450	30	90	-	-	-	VS1/VS2/VS3/VS4
650	60	90	-	-	-	VS1/VS2/VS3/VS4

separation model. Thirdly, the batch dispersion-separation model is evaluated with experimental data at two different inlet flow conditions. Fourthly, a model from [Asaadian et al. \(2022\)](#) is used to generate the drainage potential curves which are then utilized to determine the required number of tapping points to extract a fixed amount of water with an allowable total oil contamination at two inlet flow conditions. The last section presents a case study on separator design and reviews the design methodology of MPPS applied to this specific case.

3.1. Pattern map of oil/water flow in horizontal pipe

Oil field life is typically characterized by an initial period of high production rates followed by a gradual decline, ultimately leading to the end of the productive life of the field. As time passes, the water cut tends to increase, particularly in cases where enhanced oil recovery operations such as water injection are employed. Therefore, the superficial velocity of oil inside the MPPS decreases after the first year of production while the superficial velocity of water increases, eventually resulting in a decline towards the end of production. This shift in velocity leads to a change in the flow pattern from Dw/o to Do/w.

[Fig. 10](#) shows a flow pattern map of horizontal pipe flow of oil and water. The map was taken from [Trallero \(1995\)](#) using mineral oil and water with properties ($\mu_o/\mu_w = 29.6$, $p_o/p_w = 0.85$, and $\sigma = 36$ dynes/cm at 25.6°C) for 5 cm horizontal pipe diameter. Four (4) time series of superficial velocities of oil and water (V_{so} , V_{sw}) pairs has been plotted on the chart, considering that different number of branches are used in the MPPS, ranging from 1 to 8. The time series were obtained from the production profile provided in Figure 26 in the Appendix C. The superficial velocities were calculated by converting the standard conditions rates in the profile to local conditions of pressure and temperature of the separator and subsequently dividing by the area. The [Fig. 10](#) indicates that increasing the number of parallel branches in the MPPS results in a shift towards more segregated flows such as stratified flow or stratified flow with interface mixing. However, there is a tradeoff between ensuring segregated flow and cost of having too many pipes. The limitation of the pipe length can help to find the best design solution and number of branches.

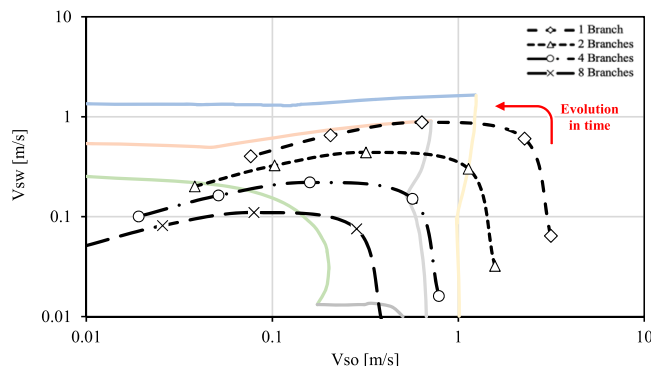


Fig. 10. Flow pattern map of production rates with different numbers of MPPS branches.

3.2. Experimental results: evolution of phases' thickness

[Fig. 11](#) shows the evolution of layer thickness for a total flow rate of 300 L/min and an extraction rate (ER) of 90 %. Four different WC_{inlet}s are shown in [Figs. 11a–11d](#). The thickness of the emulsion layer (depicted in beige color) is considerably reduced along the horizontal section for inlet water cuts (WC_{inlet}) of 50 %, 70 %, and 90 %. In contrast, the emulsion layer remains relatively stable for a 30 % WC_{inlet}. Increasing the WC_{inlet} results in a slight decrease in emulsion layer thickness at the beginning and end of the horizontal pipe (VS.1, VS.4, [Fig. 9](#)). Higher WC_{inlet}s also lead to an increase in the thickness of both the oil and brine layers due to the breakdown of the emulsion layer. Water layers are generally thicker for high WC_{inlet}s (e.g., 70 % and 90 %) and thinner for low WC_{inlet}s. The residence time for a total flow rate of 300 L/min is estimated to be 20 seconds, which is sufficient to separate the emulsion layer for the highest WC_{inlet} of 90 %, but not enough thus resulting in a thick oil/emulsion layer for the lowest WC_{inlet} of 30 %.

Similar results are obtained for other two total flow rates 500 and 700 L/min. Detailed discussions related to mentioned flowrates are presented in Appendix D.

3.3. Experimental results: variation of the water cut of the emulsion layer (WC_E) along the MPPS

[Fig. 12](#) shows how the water cut in the emulsion layer (WC_E) changes along the MPPS as a function of different WC_{inlet} values (30 %, 50 %, 70 %, and 90 %) and three different total flowrates (300, 500, and 700 L/min). The WC_E was measured and recorded along the MPPS from the inlet towards the sampling points SP.1, SP.2, and SP.3. The inversion point was observed at approximately 32 % WC_{inlet}, the behavior of WC_E variation differs when WC_{inlet} equals 30 % compared to other measured inlet water cuts (WC_{inlet}). Specifically, the emulsion type for this flow condition is WiO, whereas for the remaining WC_{inlets}, the emulsion system is OiW. [Fig. 12a](#) depicts the changes in WC_E for a total flowrate of 300 L/min. The WC_E decreases from the inlet (SP.1) to the beginning of the horizontal section (SP.2) for all WC_{inlet} conditions. This trend is reversed when the oil-water mixture moves from the beginning of the horizontal section (SP.2) to the end of it (SP.3), resulting in a higher final WC_E than the initial WC_E for all WC_{inlet} conditions. The WC_E exhibits similar values for WC_{inlet} conditions of 30 % and 50 %. Increasing WC_{inlet} values result in higher WC_E values.

[Fig. 12b](#) presents similar plots as 12a for a total flowrate of 500 L/min. As expected, the flow conditions with a higher WC_{inlet} lead to a higher WC_E at the inlet (SP.1). The WC_E then decreases as the oil-water mixture moves towards the beginning of the horizontal section (SP.2). However, as the mixture reaches the end of the horizontal section (SP.3), the flow conditions with a lower WC_{inlet} exhibits a higher WC_E, which is opposite to what all other curves for inlet water cuts greater than 30 % exhibit. In [Fig. 12c](#), when the total flow rate is 700 L/min, the variation of WC_E along the MPPS is modest. When there is a water-continuous flow pattern at the inlet (e.g., WC_{inlet} 70 and 50 %) the WC_E decreases along the separator. Based on the results shown in [Fig. 11](#), there is separation occurring between the sampling sections (SP.1) towards section (SP.3), i.e., the sedimentation layer is shrinking and the dense-

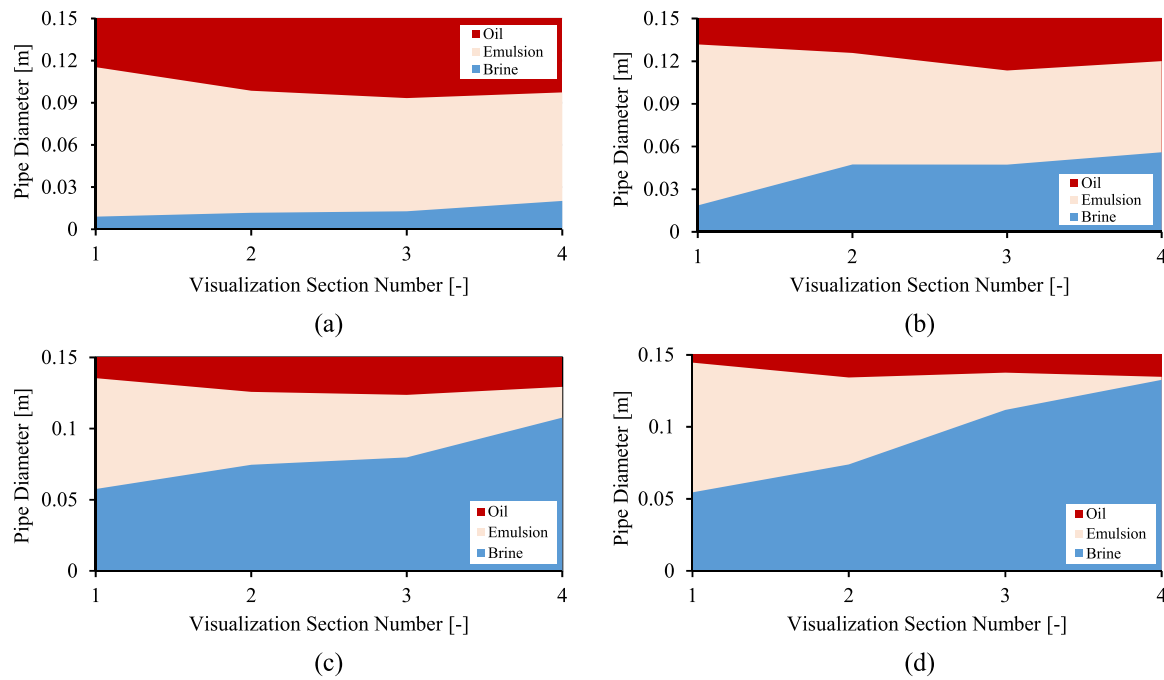


Fig. 11. Evolution of phase thickness for a total flow rate of 300 L/min, an extraction rate (ER) of 90 % and WC_{inlets} a)30 %, b)50 %, c)70 % and d)90 %. The water layer is depicted with blue color, the oil in red and the emulsion layer in beige.

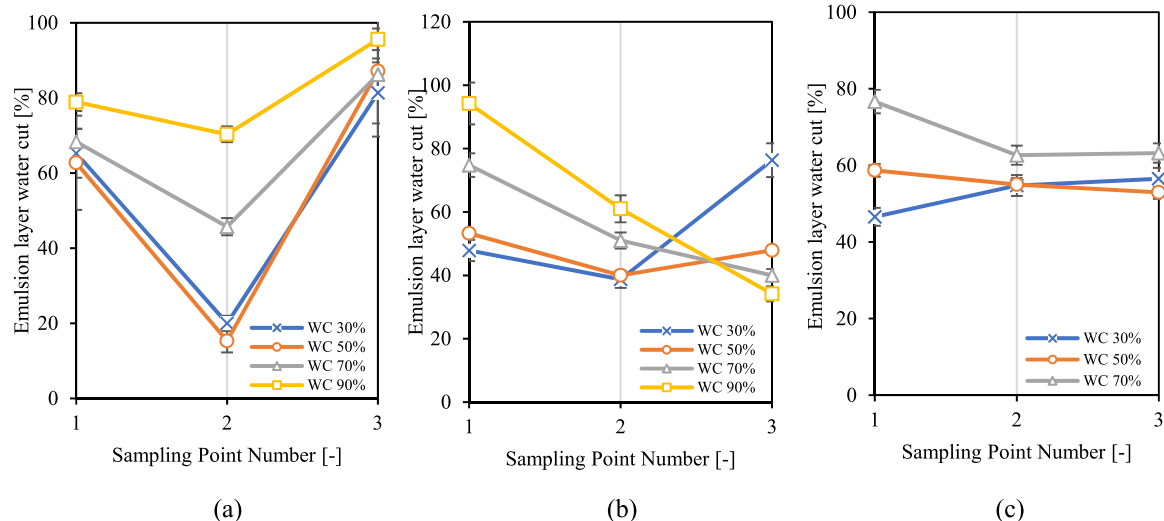


Fig. 12. Water cut alteration in the emulsion layer as a function of different WC_{inlet} values (30 %, 50 %, 70 %, and 90 %) and total flowrates a)300, b)500, and 700 L/min.

packed layer with lower water cut is growing. However, the length of the horizontal section is not sufficient to observe full separation and thus a considerable alteration in WC_E. The same observation applies to the WC_{inlet} 30 % with the difference that the WC_E only increases slightly.

3.4. Experimental results: Droplet size distribution (DSD)

This subsection presents the droplet size distribution for each flow condition measured at each sampling point. A sensitivity analysis on the droplet count was conducted and it was found that a minimum of 250 droplets was required for convergence of the frequency analysis.

Fig. 13a illustrates the DSD curves for flow conditions with a total flow rate of 300 L/min at MPPS inlet and WC_{inlets} of 30 %, 50 %, 70 %, and 90 %. As shown in Figs. 13b-13f, the highest WC_{inlet} of 90 % produced the most uniformly dispersed droplets compared to other

WC_{inlet}s. However, the droplet size at the WC_{inlet} of 50 % was larger than for other flow conditions. A higher fraction of dispersed phase can promote droplet coalescence and the formation of larger droplets, as reflected in the Sauter mean diameter measurements in Fig. 13b (Asaadian & Stanko, 2023). When comparing the Sauter mean diameter of WC_{inlets} at 30 % and 70 %, it is evident that the OiW emulsion produces a more dispersed flow than the WiO emulsion with the same fraction of dispersed phase.

Figs. 14a-14c depict the Sauter mean diameter for various flow conditions as per the test matrix (Table 1). Fig. 14a illustrates the mean droplet diameter at the MPPS inlet (SP.1). The low total flowrate leads to a larger mean diameter of droplets due to a reduction in the shear force, which is the primary force responsible for emulsifying the oil and water phases in the pipe. Conversely, an increase in the total flowrate leads to a reduction in the Sauter mean diameters for all WC_{inlet}s. At high total

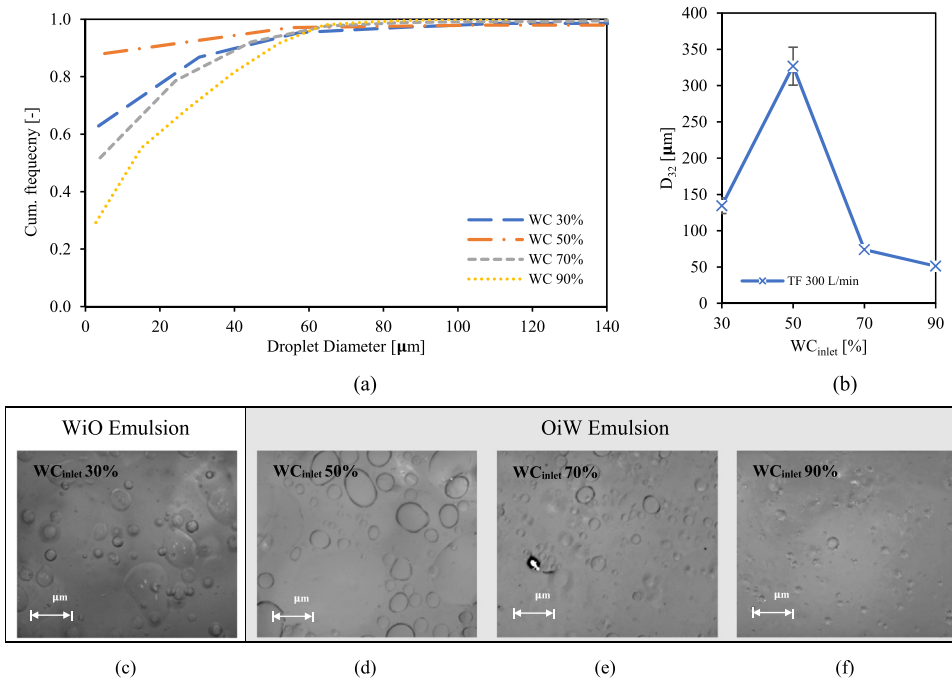


Fig. 13. a)Droplet size distribution analysis of the flow with total flow rate of 300 L/min at the MPPS inlet, b)Sauter mean diameter vs. WC_{inlet} and microscopic images of emulsion layer at WC_{inlet}s c)30, d)50, e)70 and f)90 %.

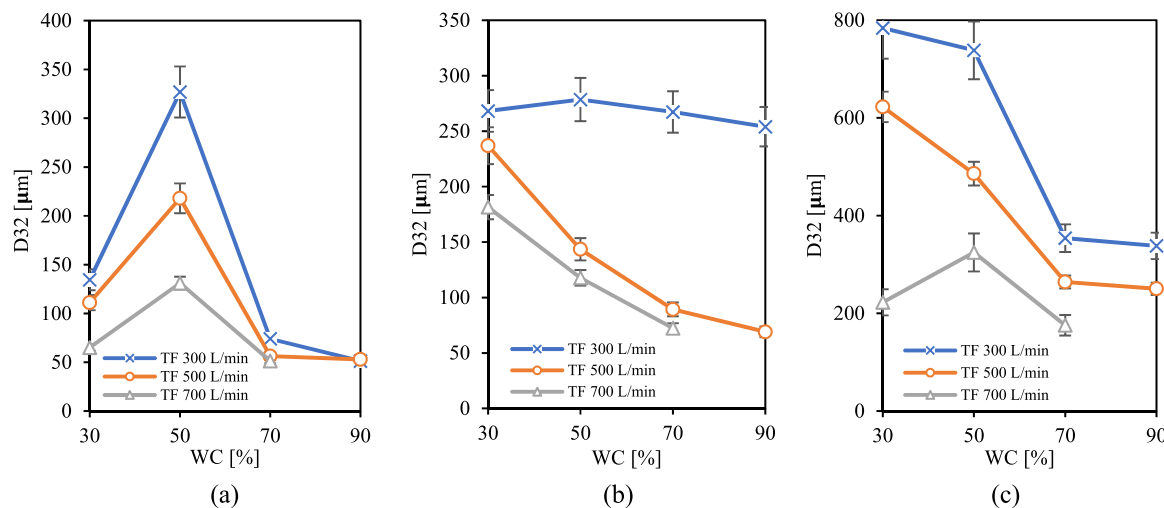


Fig. 14. Sauter mean diameter measurements at a)SP.1, b)SP.2 and c)SP.3.

flowrates (e.g., 500 L/min), changing the WC_{inlet} from 70 % to 90 % does not result in a significant change in the mean droplet size at a given position inside the separator.

It should be noted that the inversion point in the tested fluid system occurs at a 32 % water cut. Consequently, the quantities and trends of the Sauter mean diameter for water cuts ranging from 50 % to 90 % pertain to the OiW emulsion system, whereas the values for a 30 % water cut correspond to the WiO emulsion system. This distinction explains the inflection point observed in Fig. 14a. Comparing the Sauter mean diameters of the WiO and OiW emulsion systems at the same dispersed fraction reveals that the WiO emulsion results in larger dispersed droplets due to the stronger surface forces of saltwater compared to Exxsol D60.

Fig. 14b displays the Sauter mean droplet diameters measured at the end of the downward-inclined section (SP.2, at the beginning of the horizontal section). A slight decrease in mean droplet size is observed in

the lower total flowrate of 300 L/min with an increase in WC_{inlet}. However, with higher total flowrate, an increase in WC_{inlet} leads to a drop in the Sauter mean diameter. The Sauter mean diameter measurements at the end of the horizontal section (SP.3) are presented in Fig. 14c. As seen in the previous figures, the mean droplet size reduces with an increase in the total flowrate. Although there is not a significant difference between the mean droplet sizes of WC_{inlet}s 70 % and 90 % in the two total flowrates of 300 and 500 L/min. The rate of Sauter mean diameter growth decreases with increasing the inlet flow rate, hence it provides less residence time.

Fig. 15a shows the variation of the droplet size distribution curve in the MPPS for a total flow rate of 500 L/min and WC_{inlet} 90 %. There are smaller droplets and more uniform distributions at the MPPS inlet, and larger droplets at the end of the horizontal section. Fig. 15b shows the measured Sauter mean diameter, indicating that droplets coalesced and formed larger droplets from SP.1 towards SP.3. The growth in the mean

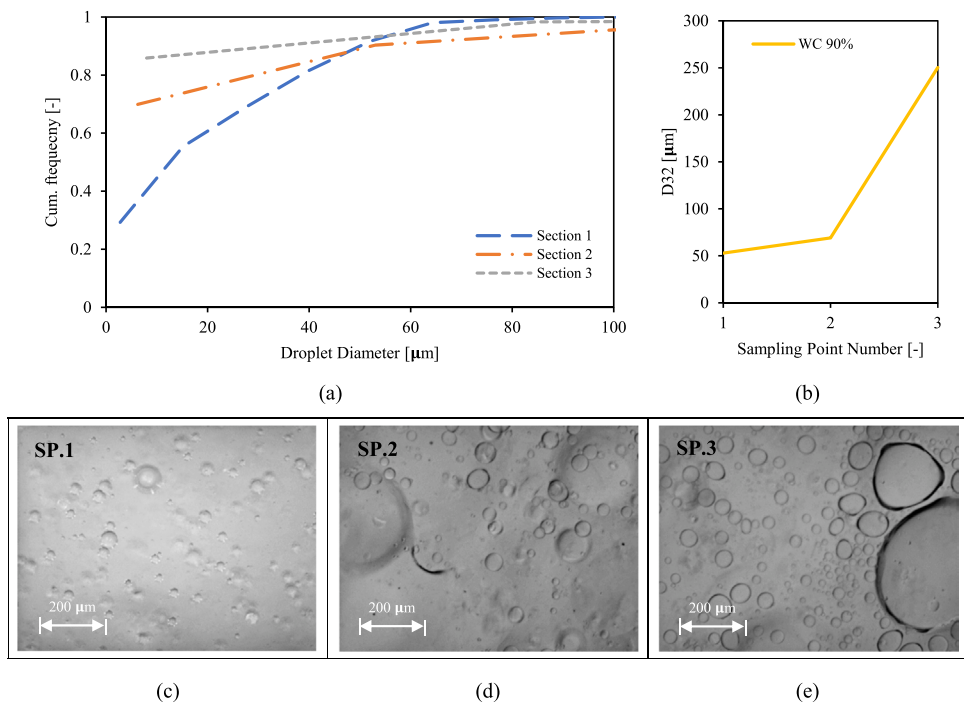


Fig. 15. a)Droplet size distribution analysis of the flow with total flow rate of 500 L/min and WC_{inlet} 90 %, b)Sauter mean diameter vs. sampling point locations and microscopic images of the emulsion layer at c)SP.1, d)SP.2, and e)SP.3.

droplet size is more significant in the flow from SP.2 towards SP.3, as demonstrated in microscopic images presented in Figs. 15c–15e.

The variation of the measured Sauter mean droplet diameters along the MPPS for different flow conditions are presented in Fig. 16. In general, there is an increase in droplet size from the inlet (SP.1) towards the end of the horizontal pipe section (SP.3). However, in WC_{inlet} 50 %, a decrease in the mean droplet diameter occurred from SP.1 towards SP.2. When comparing the Sauter mean diameter values for different total flow rates of 300, 500, and 700 L/min, it seems that the high mixture velocities do not provide the emulsion layer with enough residence time for droplet coalescence.

3.5. Batch dispersion-separation model validation

The experimental data obtained were utilized to validate and tune the batch dispersion-separation model for the MPPS. The asymmetric dimple parameter (r_V^*) was manually set to 9.5 E-04 to achieve the exact phases thickness in pipe according to inlet water cut after the complete separation in pipe. As shown in Fig. 17, the model and experimental data exhibit reasonable agreement for an inlet flow condition with a total flow rate of 300 L/min and a WC_{inlet} of 50 %. The effective length (L_{eff}) of the horizontal pipe section of MPPS is 3.7 m. The prediction of the model matched the reported experimental data when the separation process is set to start at an axial position of 6 m. At the beginning of the horizontal section, thin layers of oil and water single phases were visible due to partial separation in the descending pipe section.

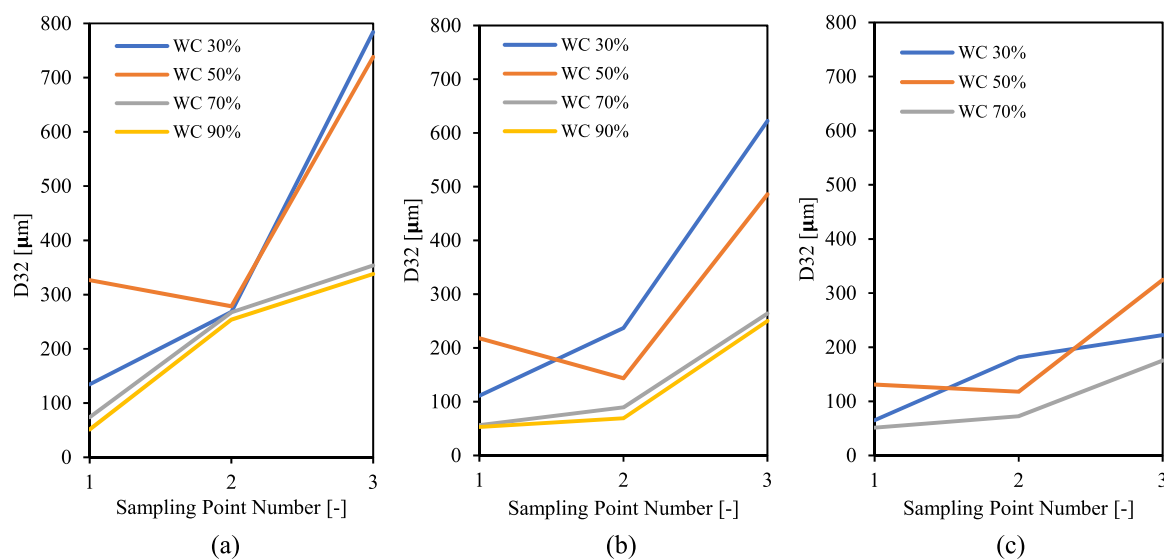


Fig. 16. Sauter mean diameter measurements at total flowrate a)300, b)500 and c)700 L/min.

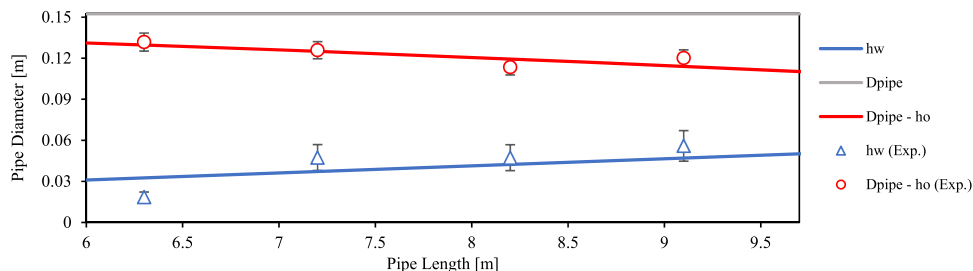


Fig. 17. Comparison between model prediction and experimental data for total flowrate 300 L/min and WC_{inlet} 50 %.

Fig. 18 compares the data matching model results with the experimental data points from flow condition total inlet flowrate 500 L/min, WC_{inlet} 30 %. The matching result confirms the model output with the same asymmetric dimple parameter (r_1^*) 9.5 E-04 with the lower WC_{inlet} and the higher total inlet flowrate. In this case, the model prediction matches the experimental data when the separation process begins at the fourth meter of the model pipe length.

3.6. Drainage Potential Curve Study

In this subsection, a tapping design analysis for the tapping point of the MPPS is done for two inlet flow conditions, 1) total flowrate 450 L/min, WC_{inlet} 30 % and 2) total flowrate 650 L/min, WC_{inlet} 60 %. These two inlet flow conditions lie on the edge of the sufficient separation performance envelope of the MPPS resulted from the previous work, Asaadian and Stanko (2023). They are selected to show how delicately the methodology will perform under challenging conditions. It is assumed that it is desirable to drain 80 % of the inlet water flow through the tapping points (variable name is WT). The design analysis is done by performing interpolation on data points measured in previous experimental campaigns in Asaadian et al. (2022). New experimental data gathered in the present work is utilized to validate the drainage potential curve method. This subsection aims to achieve two goals: firstly, to demonstrate the effectiveness of the approach within the tapping point design stage of the methodology by employing the experimental results from test campaign, and secondly, to assess the reliability of the developed model, validated by experimental data, for integration into the design methodology.

Figs. 19a-19c shows the production potential curves of each tapping point with the operating value pair of water cut of tapped stream (WC_{tapped}) and water fraction of inlet water flow drained (WT). The lines are values obtained using bi-linear interpolation using experimental data obtained in earlier studied (Asaadian et al. 2022). Since the geometry of the tapping point and separator, and fluid properties are fixed, it is assumed that the drainage potential curve depends only on the water cut of the inlet stream and the total flow rate. The points (symbols) in colors other than red are values measured experimentally. The curves are shown when using single (a), double (b), and triple (c) tapping points for inlet flow condition of total flowrate 450 L/min, and WC_{inlet} equal to 30 %. Since the drainage potential curve of a tapping point depends on the inlet total flow rate and water cut, in multi-tapping point

arrangements, the drainage potential curves of the subsequent tapping points depend on the operating conditions of the previous. For each tapping point configuration, the amount of fluid drained by each tapping point was varied such that the amount of total oil flow drained through the tapping points is minimized.

It can be observed that there is a fair agreement between the drainage potential curve obtained by interpolation on experimental data and the actual drainage potential curve.

Fig. 19d shows the total (cumulative) water fraction tapped (in % from the inlet water flow) when progressing through the tapping points. Fig. 19e shows the total (cumulative) concentration of oil in the drained stream when progressing through the tapping points. When using a single tapping point, Figs. 19a and 19e show that WC_{tapped} is equal to 77 % and oil contamination is equal to 33 gr/L.

If the second tapping is added to the separator design in the next stack, the drainage potential curve of the added tapping point is displayed in Fig. 19b. Since the inlet flow stream of the second tapping point has a lower flowrate, its performance has improved. In this case, 36 % of the inlet water phase is extracted from the first tapping point and the rest is separated at the second tapping point to reach 80 % of the inlet water rate. The water cut of the tapped stream through both tapping points is lower than the one obtained with a single tapping point. The total oil contamination in the separated stream is 18 gr/L which is significantly smaller than the value obtained with a single tapping point design.

The presence of the third tapping point and its effect on water separation is shown in Fig. 19c. The three tapping point configuration gives better performance than designs using one or two tapping points. A WT of 24 %, 26 % and 30 % are extracted from the first, second and third tapping points, respectively (Fig. 19d). The third tapping point has a better separation performance (the drainage potential curve is above that of tapping point one and two) i.e., allows to tap more water with a lower oil fraction. The total tapped water stream has a concentration of 12 gr/L oil which is less than the design using one or two tapping points (Fig. 19e). Therefore, it is found that using three tapping points is the most suitable design for tapping 80 % of the inlet water for flow conditions of 450 L/min total flowrate and WC_{inlet} 30 %.

The tapping point design for the inlet conditions of 650 L/min, WC_{inlet} 60 % is presented in detail in Appendix E.

The results from the drainage potential study revealed that the optimal number of tapping points depends on the total inlet flowrate and

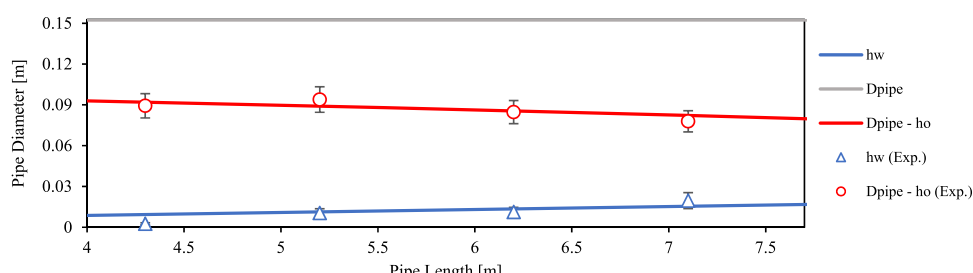


Fig. 18. Comparison between model prediction and experimental data for total flowrate 500 L/min and WC_{inlet} 30 %.

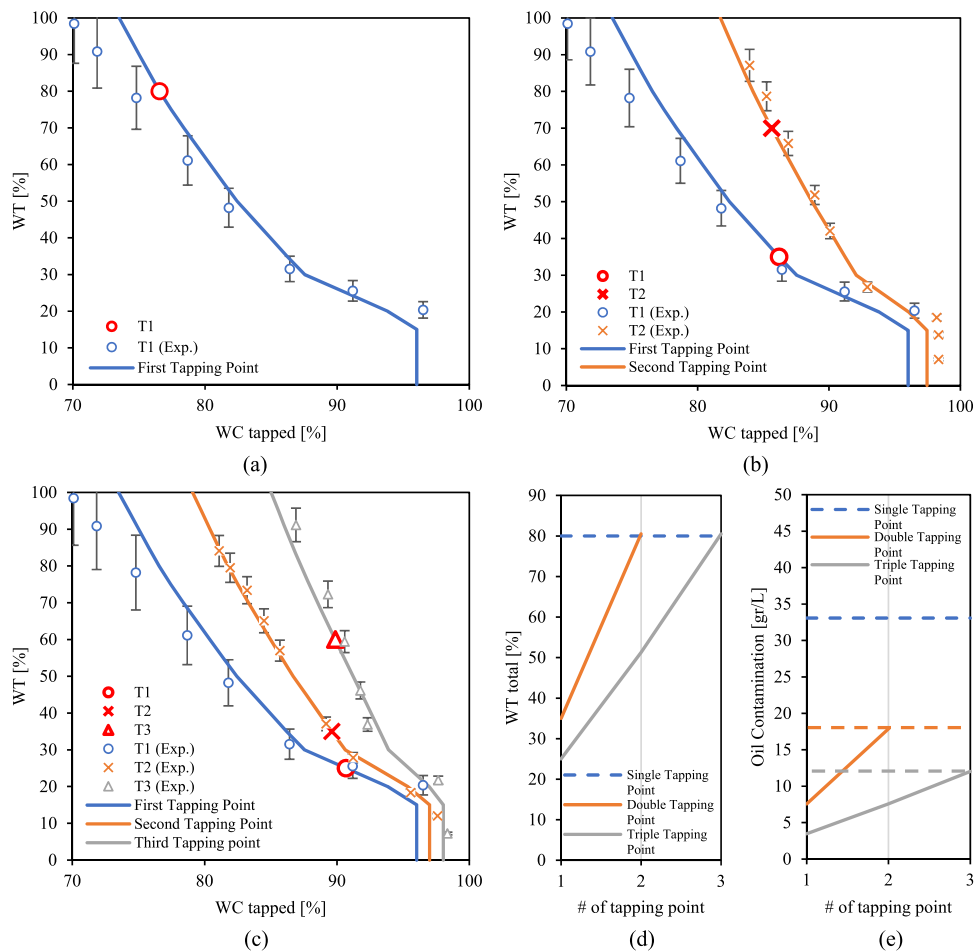


Fig. 19. Performance of water extraction from flow with a total flowrate 450 L/min and WC_{inlet} 30 by a)single, b)double, c)triple tapping points, d)water tapped and e)oil contamination from each tapping solution.

water cut. When the inlet water cut is low adding more tapping points helps to extract a certain amount of water phase with a higher water cut. However, when the inlet water cut is not too low, extracting moderate WT is possible to be done with fewer tapping points. Still, for gaining higher WT more tapping points are required.

3.7. MPPS Design Example

In this part of the study, the MPPS is designed for an offshore oil field in the North Sea. The production history and forecast of the field is illustrated in Fig. 20. During the field life, the total production rate of liquid increases gradually until year 4 and then slowly decreases. At year 7, production enhancement operations are attempted to increase the

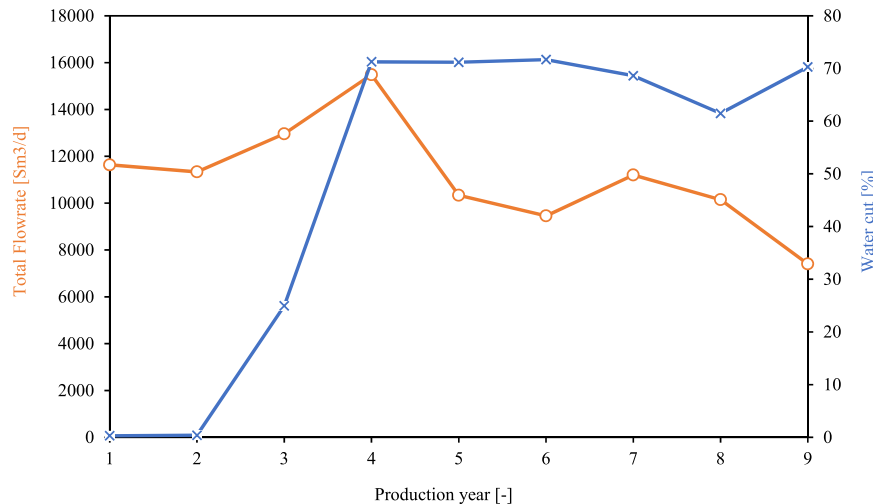


Fig. 20. Production and water cut forecast of the under-study field.

production rate. The amount of water cut increases significantly in year 4 and then it remains roughly constant. The initial droplet size and experimental asymmetric dimple parameter are considered $d_{32} = 375 \mu\text{m}$ and $r_V^* = 9.5 \times 10^{-4}$. MPPS design criteria for the studied oil field assume a total WT 80 % with a maximum fraction of 5 % oil in tapped water.

The first design task is to determine the inner diameter and number of branches to employ. For this purpose, a liquid-liquid flow pattern computational tool is used (OLGA multiphase toolkit software, version 2020.1). The aim is to vary inner diameter and number of branches to achieve segregated flow regimes (such as stratified flow with mixing in the interface (ST & MI) or stratified flow with dispersion in water (Do/w & w)). Fig. 21 shows an example flow pattern map for oil and water flow, where the regions of segregated and dispersed flow are separated by a blue line for a pipe diameter of 0.3 m. The conversion method of standard condition to local conditions about the superficial velocity is given in the Appendix F.

Since the rates of oil and water will change through the lifetime of the field, as shown in Fig. 20, the procedure described above was performed for all years in the production profile. It was assumed that the effect of fluid compressibility is negligible and that the oil contains no gas dissolved, therefore the rates at standard conditions reported in Fig. 20 are equal to the local volumetric rates at separator conditions. It was found that using an internal diameter of 0.3 m and employing four branches is sufficient to have superficial velocities that give a segregated flow pattern. The pairs of superficial velocities of oil and water for all years are plotted in Fig. 21.

The second step is to determine the required number of tapping points and the operating conditions (flow rate to tap from each tapping point). For this task, it is required to first compute the drainage potential curves of the tapping points. This needs implementation of the described methods in Section 2.2 (batch dispersion-separation model), that calculates the thicknesses of the oil, dispersion and water layers at the tapping point and Section 2.3 (drainage potential) that calculates the tapping point drainage potential from the layer thicknesses.

Since the pairs of superficial velocities of oil and water for the fourth year of production is placed near to the transition line between dispersed and segregated flow pattern, the tapping point design is performed for this year with the highest flowrate (year 4). Figs. 22a and 22b illustrate the initial water separation for the first series of four parallel branches. In each branch, the superficial velocities of oil and water are 0.18 and 0.44 m/s, respectively. It is equivalent to 1050 L/min total flowrate with 71 % WC_{inlet1} . The separation profile along the horizontal section, obtained with the batch dispersion-separation model is shown in Fig. 22a. A thin layer of oil and water are formed at the end of the horizontal pipe section and the dispersion layer occupies 80 % of the pipe diameter. Also, it is predicted that the water layer contains a 2 % volume fraction of oil. The obtained outcome from the batch dispersion-

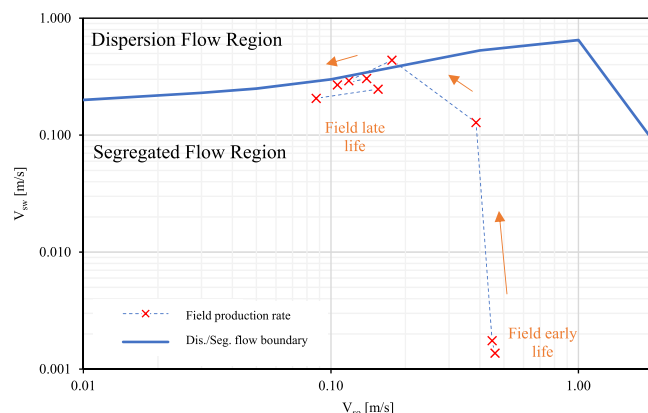


Fig. 21. Flow pattern map of the forecasted produced flow from the studied oil field.

separation model is used to generate the drainage potential curve presented in Fig. 22b. If a single tapping point is used, it is possible to extract 80 % of total inlet water with a WC_{tapped} of 82 % (orange lines and circle in Fig. 22b).

If a second tapping point is employed, then it is possible to drain from the first tapping point 48 % of the total inlet water with a water cut of 95 % (red lines and circle in Fig. 22b). This amount of water is equal to 357.8 L/min of the total inlet water rate of 745.5 L/min. The second tapping point will operate with the remaining flow, i.e., a total flowrate of 692.2 L/min and WC_{inlet} of 58.5 %. The batch dispersion-separation model is run again with this input. Since the flowrate is decreased the layers of oil and water at the end of the horizontal branch are thicker than in the horizontal section that approaches the first tapping point. In this case, the transition layer occupied 53 % of the pipe diameter, and no oil contamination is predicted in the water layer (Fig. 23a). As it is shown in Fig. 23b with the drainage potential curve for the inlet flow condition, 67 % of the water inlet rate can be extracted with only 5 % of the oil volume fraction (95 % WC_{tapped}). This means the second round of water separation is able to extract 271.8 L/min of water phase and overall, 84.4 % total WT.

Total oil contamination rate is 107.3 and 31.4 L/min for single and double tapping point solutions respectively. This shows adding the second tapping point and stack significantly decreases the oil contamination rate in water outlet line. Therefore, the final MPPS design for the studied oil field is an MPPS with 2 series of 4 parallel branches with a pipe diameter of 0.3 m. The changes of each phase flow rate after each stage of extraction in of MPPS are illustrated in Fig. 24.

4. Conclusions

Based on this study, the following conclusions have been drawn:

- A new MPPS model-based design methodology has been proposed. The models are described in detail and validated with experimental data and an example case is described to illustrate the methodology. The design methodology consists of the following steps:
 - Determining the MPPS pipe diameter and number of branches using the inlet flow rates of oil and water and a flow pattern prediction tool. The MPPS pipe diameter and number of branches are set such that segregated flow regimes are achieved in the separator pipe branches.
 - Determining the number of tapping points and the flow rates drained by each tapping point. This task is performed by using tapping point drainage potential curves and testing different combinations of tapped flow rates and tapping points that give highest amount of water drained with lowest content of oil. The tapping point drainage potential curves are calculated as follow:
 - The evolution of the thickness of the three layers (water, oil, and emulsion) along the horizontal section approaching a tapping point is forecasted by using a batch dispersion-separation model. The model has been modified and adapted from models discussed in the literature with asymmetric dimple parameter (r_V^*) 9.5×10^{-4} , and it was validated with extensive experimental data gathered by the authors.
 - The tapping point drainage potential curves are calculated using the layer thicknesses estimated in the previous step using the method presented in Asaadian et al. (2022). This showed when the inlet water cut is low (e.g., 30 %), adding more tapping points helps to extract the water phase with a higher water cut. However, when the inlet water cut is higher (e.g., 60 %), moderate water cut can be achieved with fewer tapping points.
 - An offshore oil field was utilized to test the suggested methodology, and the resulting MPPS design, an MPPS with 2 series of 4 parallel branches with a pipe diameter of 0.3 m, is documented. The chosen design prevents any flow pattern rather than segregated flow regime

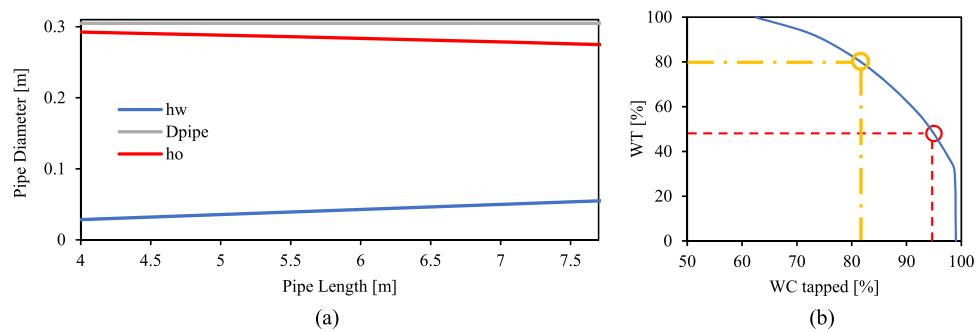


Fig. 22. Prediction of water a)separation and b)extraction from the first stack of MPPS.

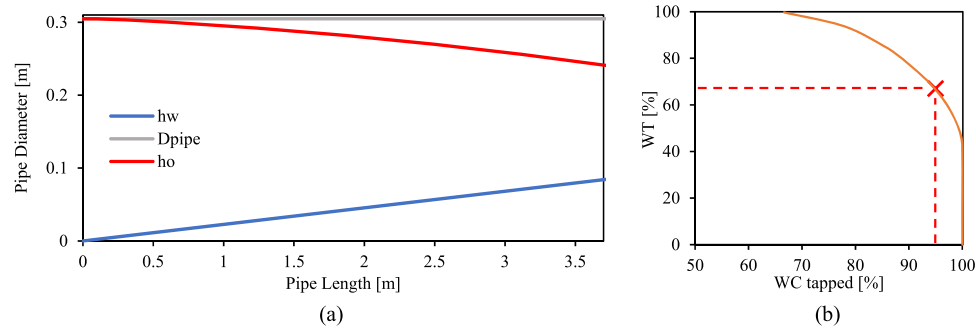


Fig. 23. Prediction of water a)separation and b)extraction from the second stack of the MPPS.

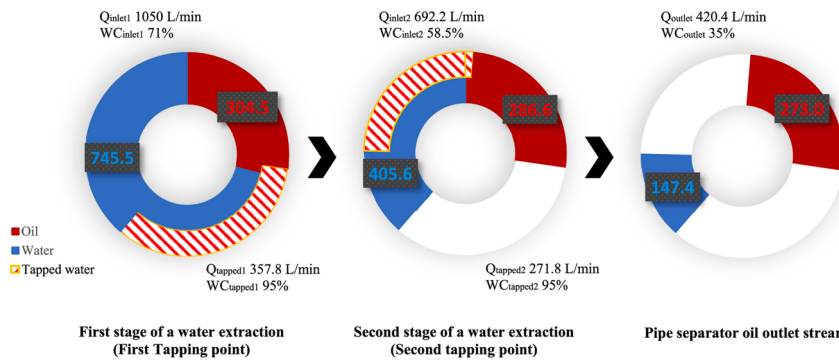


Fig. 24. Alteration of phases flow rate after each stage of extraction.

and grantee to extract 80 % total water phase with a maximum fraction of 5 % oil in tapped water.

The following recommendations outline potential areas for further investigation:

- Investigating the potential application of combining pipe separators (for bulk water separation) with hydrocyclones (for water polishing) subsea.
- Comparison between the batch dispersion-separation model and the population balance model and general improvement of the design methodology.

CRediT authorship contribution statement

Hamidreza Asaadian: Conceptualization, Data curation, Formal

analysis, Investigation, Methodology, Software, Validation, Visualization, Writing – original draft. **Milan Stanko:** Conceptualization, Funding acquisition, Methodology, Project administration, Resources, Supervision, Writing – review & editing.

Acknowledgement

The authors gratefully acknowledge the financial contributions made by the Research Council of Norway, the Department of Geoscience and Petroleum at NTNU, and key industry partners towards SUBPRO, a research-based innovation center for subsea production and processing. This work was conducted under project number 237893 as a part of SUBPRO.

Appendix A

Sedimentation Curve Analysis. Separating oil and water mixtures is first accomplished by gravity sedimentation and flotation. The sedimentation analysis proposed here is as follows: For the inclusion of droplet internal flow circulation, Pilhofer and Mewes (1979) proposed several dimensionless parameters. Parameters such as the Archimedes number (Ar), friction coefficient (C_W), Hadamard-Rybczynski factor (K_{HR}), Reynolds number of droplets in an infinite fluid (Re_∞) and dispersed-phase viscosity and other parameters ξ and λ are also included.

$$Ar = \frac{\rho_c - \rho_d}{\mu_c^2} \frac{d_p^3}{\Delta \rho g} \quad (A1)$$

$$\xi = 5K_{HR}^{-3/2} \left(\frac{\phi}{1-\phi} \right)^{0.45} \quad (A2)$$

$$K_{HR} = \frac{3(\mu_c + \mu_d)}{2\mu_c + 3\mu_d} \quad (A3)$$

$$\lambda = \frac{1 - \phi}{2\phi K_{HR}} \exp \left(\frac{2.5\phi}{1 - 0.61\phi} \right) \quad (A4)$$

$$C_W = \frac{Ar}{6Re_\infty^2} - \frac{3}{K_{HR} Re_\infty} \quad (A5)$$

$$Re_\infty = \frac{\rho_c v_s^\infty d_p}{\mu_c} = 9.72 \left[(1 - 0.01Ar)^{4/7} - 1 \right] \quad (A6)$$

The slip velocity is defined as:

$$v_s = \frac{3\lambda\phi\mu_c}{C_W\xi(1-\phi)\rho_c} \frac{d_p}{d_p} \left[\left(1 + Ar \frac{C_W \xi (1-\phi)^3}{54 \lambda^2 \phi^2} \right)^{0.5} - 1 \right] \quad (A7)$$

The evolution of a water single phase layer (sedimentation curve) can be predicted by Eq. A8, which takes into account the fluid properties of the mixture.

$$h_w = \frac{v_s x}{u_m} \quad (A8)$$

Coalescence Analysis. The oil droplets migrate to the top of the pipe, where they coalesce to create the oil layer of thickness h_o . The coalescence of droplets with a flat interface determines the rate of change of h_o with respect to time. Pereyra (2011) established that the rate of change of the oil circular cross-sectional area is determined in Eq. A9 by assuming that all droplets at the interface have the same diameter and use the shape shown in Fig. 4. Droplet diameter is determined by the Sauter mean diameter (d_{32}^i) at the separator inlet for settling velocity.

$$u_M \frac{dh_o}{dx} = \frac{2\phi_i d_{32}^i}{3\tau_i} \quad (A9)$$

It is assumed that the fraction of the dispersed phase at the interface is equal to unity (1), and the time evolution of the oil single-phase layer h_o is defined by Eq. A9, which can be solved numerically using an explicit scheme. To obtain a solution, it is necessary to determine the Sauter mean diameter at the interface. The dense-packed region considers binary coalescence or coalescence between two particles. Hartland and Jeelani (1988) developed an expression for estimating the evolution of droplet size as a function of droplet-droplet coalescence time (τ_c), assuming that all droplets are of the same size and are in the same vertical position throughout each time step.

$$u_M \frac{d(d_{32})}{dx} = \frac{d_{32}}{6\tau_c} \quad (A10)$$

The distribution of droplet sizes in the dense-packed zone is necessary for modeling the coalescence process. The higher the dense-packed zone, the more the droplets deform, affecting the coalescence process. The coalescence time between two droplets with the same Sauter mean diameter d_{32} is defined by Henschke et al. (2002) according to asymmetric film drainage analysis as:

$$\tau_c = \frac{(6\pi)^{7/6}}{4\sigma^{5/6}} \frac{\mu_c}{H^{1/6}} \frac{r_a^{7/3}}{r_{F,C} r_v^*} \quad (A11)$$

By modifying the previous equation, the coalescence time for a single droplet with Sauter diameter d_{32} and a flat interface will be:

$$\tau_i = \frac{(6\pi)^{7/6}}{4\sigma^{5/6}} \frac{\mu_c}{H^{1/6}} \frac{r_a^{7/3}}{r_{F,I} r_v^*} \quad (A12)$$

Henschke et al. (2002) proposed an empirical formulation for droplet deformation based on a numerical solution of droplet deformation in a dense-packed zone, where the radius of the droplet/droplet contact area is given by:

$$r_{F,C} = 0.3025 d_{32} \sqrt{1 - \frac{4.7}{La + 4.7}} \quad (A13)$$

The modified contact area radius for a droplet to interface coalescence is given by: (Burrill and Woods, 1973)

$$r_{F,I} = \sqrt{3} r_{F,C} \quad (A14)$$

and the channel contour radius is predicted from:

$$r_a = \left(\frac{|\rho_D - \rho_C|g}{\sigma} \right)^{0.6} h_p^{0.2} \quad d_{32} \quad r_{F,I} = \sqrt{3} \quad r_{F,C} \quad (\text{A15})$$

The Hamaker coefficient (H) and the asymmetry parameter (r_V^*) are both unknown parameters in Eqs. A11 and A12. Experimental settling curves are used to adjust the asymmetry parameter, which makes it unique to each system. For all systems, Henschke et al. (2002) suggested a Hamaker coefficient of 10^{-20} Nm.

As mentioned earlier, the solution of batch dispersion-separation model requires spatial and temporal discretization. The Sauter mean diameter along the dense-packed zone is predicted by spatial discretization using Eq. A10, while temporal discretization predicts the evolution of layer thickness as a function of time. The remaining closure connections required to solve the proposed method are discussed next. Since the cross-sectional area of the pipe varies vertically for the MPPS, volumes rather than levels are used to describe the model. Levels and cylinder volumes must be related through geometrical connections, if the height is lower than the pipe radius, the cross-section area of the phase layer will be as:

$$A_c = \frac{D_{\text{pipe}}^2}{4} \cos^{-1} \left(\frac{D_{\text{pipe}} - 2h_i}{D_{\text{pipe}}} \right) - \left(\frac{D_{\text{pipe}}}{2} - h_i \right) \sqrt{D_{\text{pipe}}h_i - h_i^2} \quad (\text{A16})$$

and if the height of the layer is more than the pipe radius the cross-section area of the layer is:

$$A_c = \left(h_i - \frac{D_{\text{pipe}}}{2} \right) \sqrt{D_{\text{pipe}}h_i - h_i^2} + \frac{D_{\text{pipe}}^2}{4} \sin^{-1} \left(\frac{2h_i}{D_{\text{pipe}}} - 1 \right) + \frac{\pi D_{\text{pipe}}^2}{8} \quad (\text{A17})$$

Appendix B

The sampling point features a 45-degree extension and a ball valve for control. Bar supports are in place to ensure alignment between the sampling and PVM probes at this specific angle (see Figure 25). By adjusting the probe within the extension, it's feasible to position the probe tip at specific internal heights within the pipe. The diameter of both the sampling probe and extension and the rate of valve opening are precisely set to achieve an isokinetic condition.

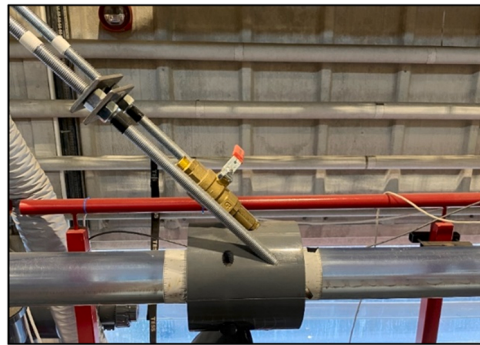


Figure 25. Sampling point of the MPPS prototype.

Appendix C

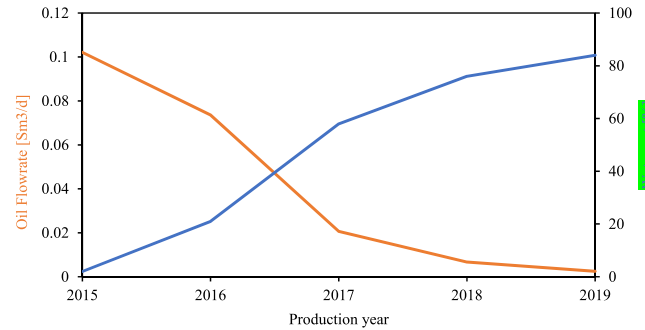


Figure 26. Production profile of an oil field.

Appendix D

Figure 27a-27d display similar plots, but with a flow rate of 500 L/min. At the end of the horizontal section, there is a slight reduction in the

thickness of the emulsion layer, but emulsion layer noticeably remains. The emulsion layer remains relatively stable for a 30 % WC_{inlet} . For WC_{inlet} s ranging from 50 % to 90 %, a noticeable clear brine layer forms at the end of the horizontal pipe (VS.4). The thickness of the formed emulsion layer is highest at VS.1 for a 90 % WC_{inlet} and decreases as the WC_{inlet} decreases. VS.4 shows a similar trend. At a total flow rate of 500 L/min, the estimated residence time is 12 seconds. To ensure a clean brine layer for a low WC_{inlet} of 30 %, a longer residence time is required.

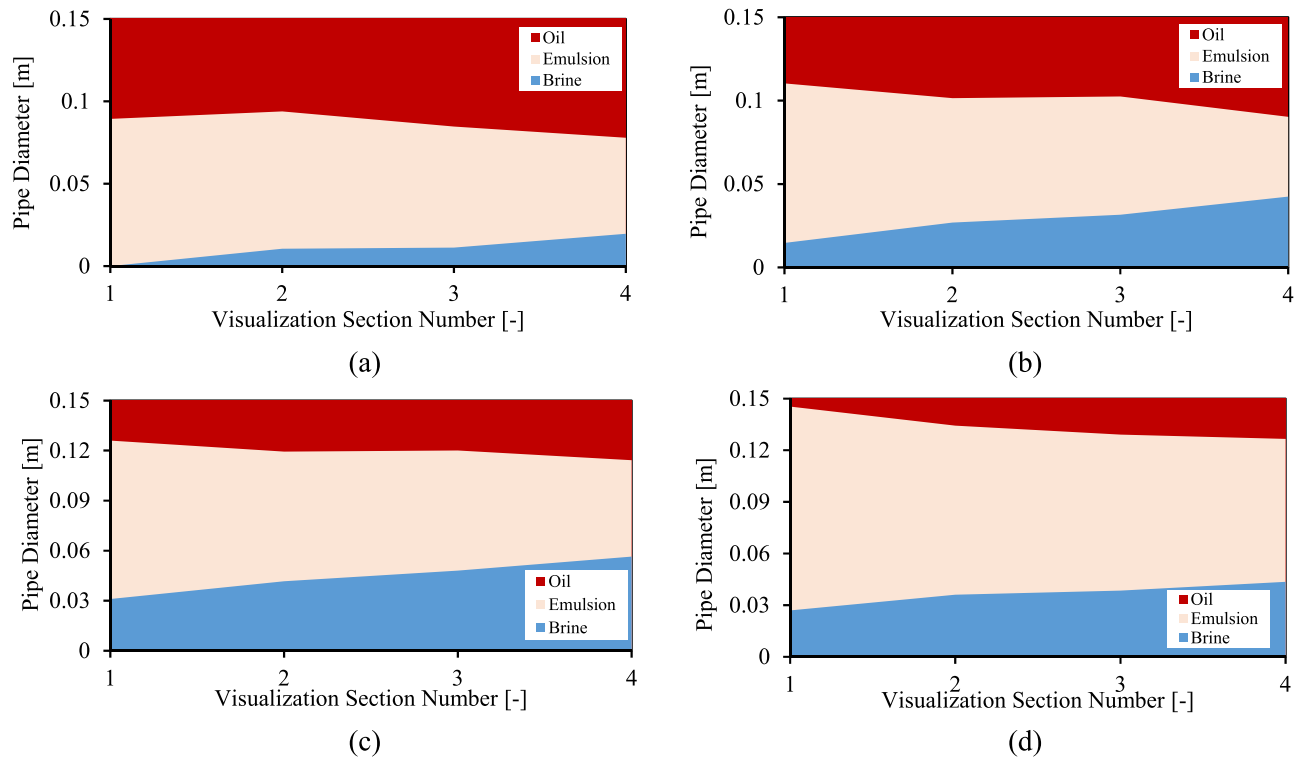


Figure 27. Evolution of phase thickness for a total flow rate of 500 L/min, an extraction rate (ER) of 90 % and WC_{inlet} s a)30 %, b)50 %, c)70 % and d)90 %.

Similar plots are shown in Figure 28 for a 700 L/min total flow rate. In the horizontal pipe section, the fluid residence time is reduced by 8 seconds as total flow rate is increased to 700 L/min. At 70 % of the WC_{inlet} s, a clean saltwater layer forms, although the thickness of the emulsion layer does not change significantly. At VS.4, the high water fraction helped create a thicker layer of clear brine because of the bouncy force. For WC_{inlet} s ranging from 50 % to 70 %, the thickness of the oil, brine, and emulsion layers is relatively stable because of the low residence time. For a WC_{inlet} of 30 %, the decrease in the emulsion layer thickness leads to an increase in the oil layer rather than the water layer.

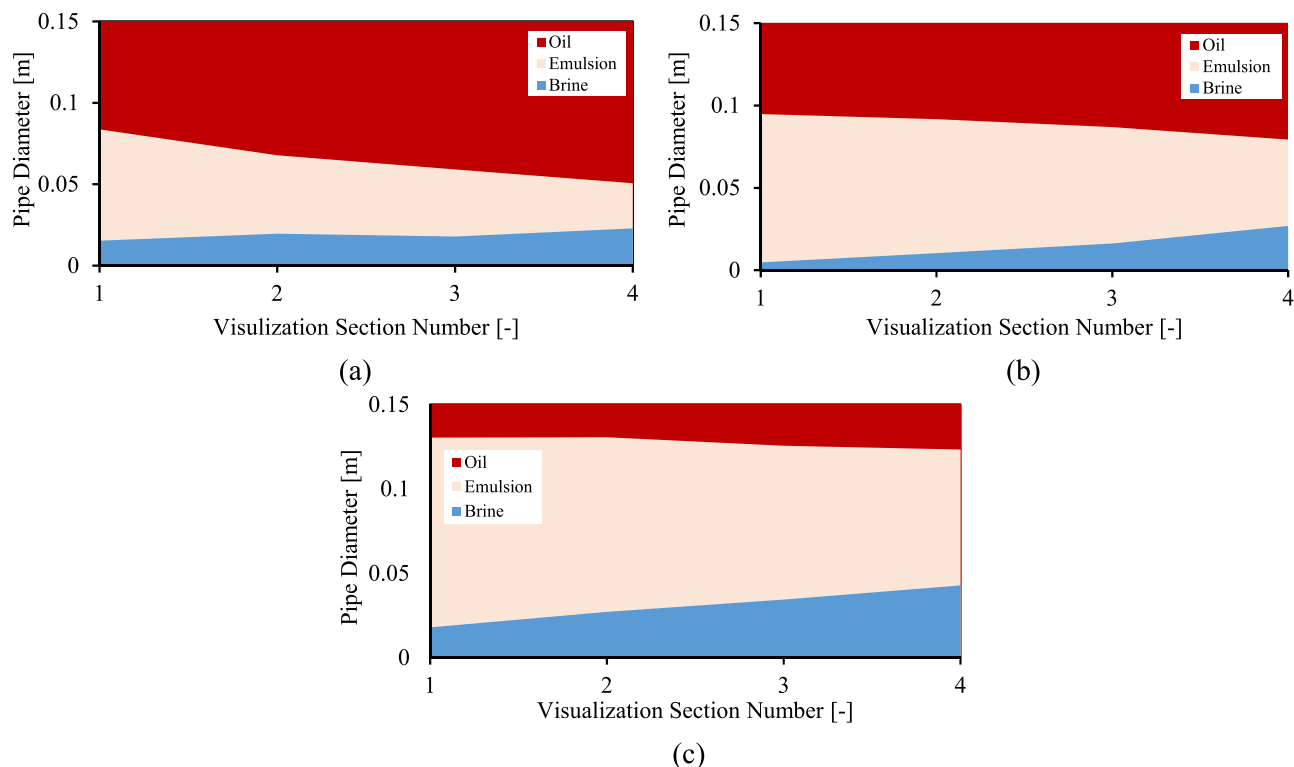


Figure 28. Evolution of phase thickness for a total flow rate of 500 L/min, an extraction rate (ER) of 90 % and WC_{inlets} a)30 %, b)50 % and c)70 %.

Appendix E

Figure 29 illustrates the performance of single, double, and triple tapping solutions for the inlet flow condition with a total flowrate 650 L/min, WC_{inlet} 60 %. As it is presented in Figure 29a, to extract 80 % water phase from a single tapping point, the tapped stream has around 80 % WC_{tapped} and will be contaminated with 75 gr/L oil phase (Figure 29e).

Adding the second tapping point helps to extract the same amount of water with significantly lower oil contamination as shown in Figure 29b and 29e. The drainage potential curve of the second tapping point shows that it is possible to extract 70 % of the inlet water stream with just 92 % WC_{tapped} which is much better than the WC_{tapped} (83 %) when using only one tapping point. The presence of a second tapping point allows to extract less water through the first tapping point, with lower oil contamination and the rest of the water phase will be extracted from the second tapping point. As it is presented in Figure 29d, 35 % of the WT is tapped from the first tapping point and the rest of that is extracted from the second tapping point so that the WT reaches 80 % totally. In this case, the total oil contamination is 26.2 gr/L which is much lower than the value obtained when using a single tapping point.

Applying the triple tapping solution at this flow condition and drainage potential curves of each tapping point is illustrated in Figure 29c. The drainage potential curve of the third tapping point has poorer performance than the second tapping in the domain of WT from 0 % to 55 % WT. As it is mentioned in Skjefstad and Stanko (2019), the performance of the tapping point is poor when the water cut in the main pipe stream is very low. After tapping water from the first and second tapping points, the water fraction is low enough to impact negatively the separation performance of the third tapping point. The overall oil contamination when the triple tapping point is applied into the system is 21.6 gr/L which is not a significant improvement.

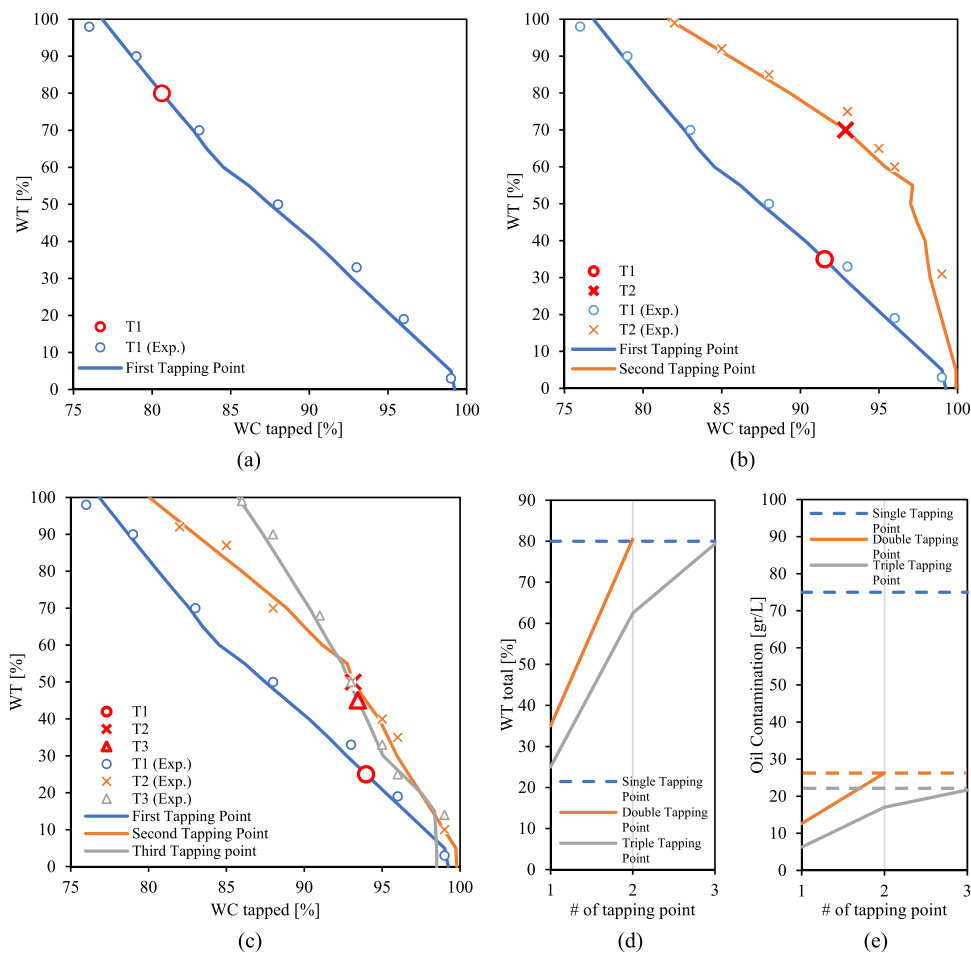


Figure 29. Performance of water extraction from flow with a total flowrate 650 L/min and WC_{inlet} 60 % by a)single, b)double, c)triple tapping points, d)water tapped and e)oil contamination from each tapping point for each tapping solution.

Appendix F

The conversion method of superficial velocity in separator from standard flow condition for oil and water is:

$$Q_t \quad [Sm^3/d] \quad \times (1 - WC) \times \frac{1d}{86400 \quad s} \quad \times \quad B_o [bbl/stb] \times \frac{1}{\pi \frac{(d_{pipe} \quad [m])^2}{4}} = V_{so} \quad [m/s] \quad (F1)$$

$$Q_t \quad [Sm^3/d] \quad \times (WC) \times \frac{1d}{86400 \quad s} \quad \times \quad B_w [bbl/stb] \times \frac{1}{\pi \frac{(d_{pipe} \quad [m])^2}{4}} = V_{sw} \quad [m/s] \quad (F2)$$

Where the B_o and B_w are oil and water formation volume factors.

References

- Asaadian, H., Harstad, S., Stanko, M., 2022. Drainage potential curves of single tapping point for bulk oil-water separation in pipe. *Energies* 15 (19), 6911.
- Asaadian, H., Stanko, M., 2023. Experimental quantification of the performance of a horizontal multi-pipe bulk separator of water and oil with crude spiking. *J. Pet. Explor. Prod. Technol.* 13 (11), 2283–2302.
- Asaadian, H., Stanko, M., 2023. Experimental characterization and evaluation of crude spiking influence on oil/water dispersed flow in pipe. *Molecules* 28 (17), 6363.
- Asaadian, H., & Stanko, M. (2023, March). An Experimental Study on the Effect of Gas on the Performance of a Multi-parallel Pipe Oil-Water Separator (MPPS). In *Gas & Oil Technology Showcase and Conference*. OnePetro.
- Assar, M., Asaadian, H., Stanko, M., Grimes, B.A., 2024. A theoretical and experimental investigation of continuous oil-water gravity separation. *Chem. Eng. Sci.* 120375.
- Bowers, B.E., Brownlee, R.F., Schrenk, P.J., 2000. Development of a downhole oil/water separation and reinjection system for offshore application. *SPE Prod. Facil.* 15 (02), 115–122.
- Burrill, K.A., Woods, D.R., 1973. Film shapes for deformable drops at liquid-liquid interfaces. II. The mechanisms of film drainage. *J. Colloid Interface Sci.* 42 (1), 15–34.
- Burrill, K.A., Woods, D.R., 1973. Film shapes for deformable drops at liquid-liquid interfaces. III. Drop rest-times. *J. Colloid Interface Sci.* 42 (1), 35–51.
- Hartland, S., 1967. The coalescence of a liquid drop at a liquid-liquid interface. Part I: Drop shape. *Trans. Instn. Chem. Engrs.* 45, 97–101.
- Hartland, S., 1967. The coalescence of a liquid drop at a liquid-liquid interface. Part II: Film thickness. *Trans. Inst. Chem. Eng.* 45, T102.
- Hartland, S., 1967. The coalescence of a liquid drop at a liquid-liquid interface. Part III: Film rupture. *Trans. Inst. Chem. Eng.* 45, 109–114.
- Hartland, S., 1969. The effect of circulation patterns on the drainage of the film between a liquid drop and a deformable liquid–liquid interface. *Chem. Eng. Sci.* 24 (3), 611–613.
- Hartland, S., Jeelani, S.A.K., 1988. Prediction of sedimentation and coalescence profiles in a decaying batch dispersion. *Chem. Eng. Sci.* 43 (9), 2421–2429.

- Hartland, S., & Jeelani, S.A.K. (1988). Prediction of sedimentation and coalescence profiles in a decaying batch dispersion. *Chemical engineering science*, 43(9), 2421–2429.
- Henschke, M., Schlieper, L.H., Pfennig, A., 2002. Determination of a coalescence parameter from batch-settling experiments. *Chem. Eng. J.* 85 (2-3), 369–378.
- Mandal, S., Bandopadhyay, A., Chakraborty, S., 2017. The effect of surface charge convection and shape deformation on the settling velocity of drops in nonuniform electric field. *Phys. Fluids* 29 (1), 012101.
- Pereyra, E.J. (2011). Modeling of integrated Compact Multiphase Separation System (CMSS (c)) (Vol. 72, No. 07).
- Pilhofer, T., & Mewes, D. (1979). *Siebboden-Extraktionskolonnen: Vorausberechnung unipulsierter Kolonnen*. Verlag Chemie.
- Sagatun, S.I., Gramme, P., Horgen, O.J., Ruud, T., & Storvik, M. (2008, May). The pipe separator-simulations and experimental results. In *Offshore technology conference*. OnePetro.
- Shi, S.Y., Xu, J.Y., Sun, H.Q., Zhang, J., Li, D.H., Wu, Y.X., 2012. Experimental study of a vane-type pipe separator for oil-water separation. *Chem. Eng. Res. Des.* 90 (10), 1652–1659.
- da Silva, F. S., Monteiro, A. S., de Oliveira, D. A., Capela Moraes, C. A., & Marins, P. M. (2013, October). Subsea versus topside processing-conventional and new technologies. In *Offshore Technology Conference Brasil* (pp. OTC-24519). OTC.
- Skjefstad, H.S., Dudek, M., Øye, G., Stanko, M., 2020. The effect of upstream inlet choking and surfactant addition on the performance of a novel parallel pipe oil-water separator. *J. Pet. Sci. Eng.* 189, 106971.
- Skjefstad, H.S., Stanko, M., 2019. Experimental performance evaluation and design optimization of a horizontal multi-pipe separator for subsea oil-water bulk separation. *J. Pet. Sci. Eng.* 176, 203–219.
- Skjefstad, H. S., & Stanko, M. (2018, October). An experimental study of a novel parallel pipe separator design for subsea oil-water bulk separation. In *SPE Asia Pacific Oil and Gas Conference and Exhibition* (p. D012S031R006). SPE.
- Skjefstad, H. S., Stanko, M., 2017, June. Subsea water separation: a state of the art review, future technologies and the development of a compact separator test facility. In: *BHR International Conference on Multiphase Production Technology*. BHR, p. BHR-2017.
- Stanko, M., & Golan, M. (2015, October). Simplified Hydraulic Design Methodology for a Subsea Inline Oil-Water Pipe Separator. In *OTC Brasil*. OnePetro.
- Stokes, G.G. (1851). On the effect of the internal friction of fluids on the motion of pendulums.
- Trallero, J.L. 1995. *Oil-Water Flow Patterns in Horizontal Pipes*. PhD dissertation, The University of Tulsa, Tulsa, Oklahoma.